Percolation and coarsening in the bidimensional voter model

Alessandro Tartaglia, Leticia F. Cugliandolo, and Marco Picco
Sorbonne Universités, Université Pierre et Marie Curie—Paris VI, Laboratoire de Physique Théorique et Hautes Energies UMR 7589, 4 Place Jussieu, 75252 Paris Cedex 05, France
(Received 7 July 2015; published 5 October 2015)

We study the bidimensional voter model on a square lattice with numerical simulations. We demonstrate that the evolution takes place in two distinct dynamic regimes; a first approach towards critical site percolation and a further approach towards full consensus. We calculate the time dependence of the two growing lengths, finding that they are both algebraic but with different exponents (apart from possible logarithmic corrections). We analyze the morphology and statistics of clusters of voters with the same opinion. We compare these results to the ones for curvature driven two-dimensional coarsening.

DOI: 10.1103/PhysRevE.92.042109 PACS number(s): 05.40.−a, 05.50.+q, 75.40.Gb

I. INTRODUCTION

Purely dynamical stochastic models are used to describe problems beyond physics such as opinion formation [1] and population genetics [2] and treat issues in ecology, linguistics, etc. In the former context, questions on the spatial spreading of opinions are posed in terms of coarsening or segregation, just as in physical materials.

The voter model [3–5] is one such purely dynamical stochastic model, used to describe the kinetics of catalytic reactions [6–8] and as a prototype model of opinion dynamics [9,10]. In its simplest realization a bivalued opinion variable, $s_i = \pm 1$, is assigned to each site on a lattice or graph with some procedure that determines the initial conditions. Typically, the initial state is taken to be unbiased, with equal number of one and the other state. The dynamic rule is straightforward: at each time step, a variable chosen at random adopts the opinion of a randomly chosen neighbor. These moves mimic the influence of the neighbourhood on the individual opinion. The probability of the chosen spin to flip in a time step is simply given by the fraction of neighbors with opposite orientation. The model is parameter free and invariant under global inversion of the spins, that is to say, $\mathbb{Z}_2$ symmetric. As a site surrounded by others sharing the same opinion cannot fluctuate, there is no bulk noise and the dynamics are uniquely driven by interfacial fluctuations. In some papers the model is defined in terms of a site-occupation variable instead of a spin.

Mathematicians, more precisely probabilists, solve this model by using a mapping to random walk theory [3,4,11]. Physicists, instead, treat it within the master equation formalism. Once written in this form, one reckons that the transition probabilities do not satisfy detailed balance and, therefore, the model is essentially out of equilibrium. Even though there is no asymptotic thermal state, the dynamics can be solved as Glauber did for the stochastic Ising chain since the equations for the correlations of different order decouple [6,8,12].

The voter model's evolution shows spatial clustering of similar opinions. It approaches one of the two absorbing states with complete consensus via a coarsening process in $d \leqslant 2$. It may also approach consensus in finite-size $d > 2$ systems but only because of a large random fluctuation with some small probability (that vanishes in the infinite-size limit). Otherwise, an infinite family of disordered steady states exists in $d > 2$ [11,13]. The coarsening process in $d = 2$ differs considerably from the curvature driven one, as can be appreciated in Fig. 1 where a series of snapshots of the spin configuration at increasing times are shown, proving that the long-term dynamics are not determined by symmetry properties alone. It also differs from critical relaxation, especially because of the lack of bulk fluctuations, see also Fig. 1.

The absence of bulk noise and surface tension entails important differences with respect to curvature-driven phase-ordering kinetics [14–16]. In the voter model, regions of one opinion can only be penetrated by the other at the boundary. Besides, a large bubble consisting of voters of the same opinion does not shrink as in curvature-driven processes. It slowly disintegrates as its boundary roughens diffusively to reach a typical width of the order of the initial radius [17,18], while the radius of the droplet remains statistically constant (the radially averaged magnetization profiles have a stationary middle point).

Coarsening processes usually conform to the dynamic scaling hypothesis [14–16]. This assumption states that if there is a single growing length in the process, say, $\ell(t)$, the statistical properties of the system are self-similar with respect to it. Under this assumption the space-time correlation is independent of time when distance is rescaled by $\ell(t)$. In the voter model the evolution of a random initial condition shows the growth of ordered spatial regions. However, the exact asymptotic solution of an *infinite system* in $d = 2$ exhibits logarithmic violations of the standard scaling forms [14]. Although a characteristic length $\ell(t) \simeq \sqrt{t}$ can be identified, the density of interfaces decays as $1/\ln t$ and the scaling function for the space-time correlation function $C(r,t)$ involves an additional logarithmically decaying factor [11] (somehow similarly to the critical dynamic scaling [19,20] though with a logarithm instead of an algebraic correction).

The goal of this work is to characterize the coarsening process in the bidimensional voter model with large but *finite linear size* by studying, in detail, the geometric and statistical properties of the dynamic pattern of domains. Following the analysis in Refs. [21–24] we will demonstrate that the system evolves in two time regimes: a preasymptotic approach to critical percolation and an ultimate approach to full consensus. With the aim of identifying and distinguishing the growing lengths in each of these regimes, we compute special time-dependent observables such as the number density of domains with a given area or the number density of interfaces with a given length. As the characteristic length associated to the approach to percolation, which we call $\ell_P(t)$, grows quite

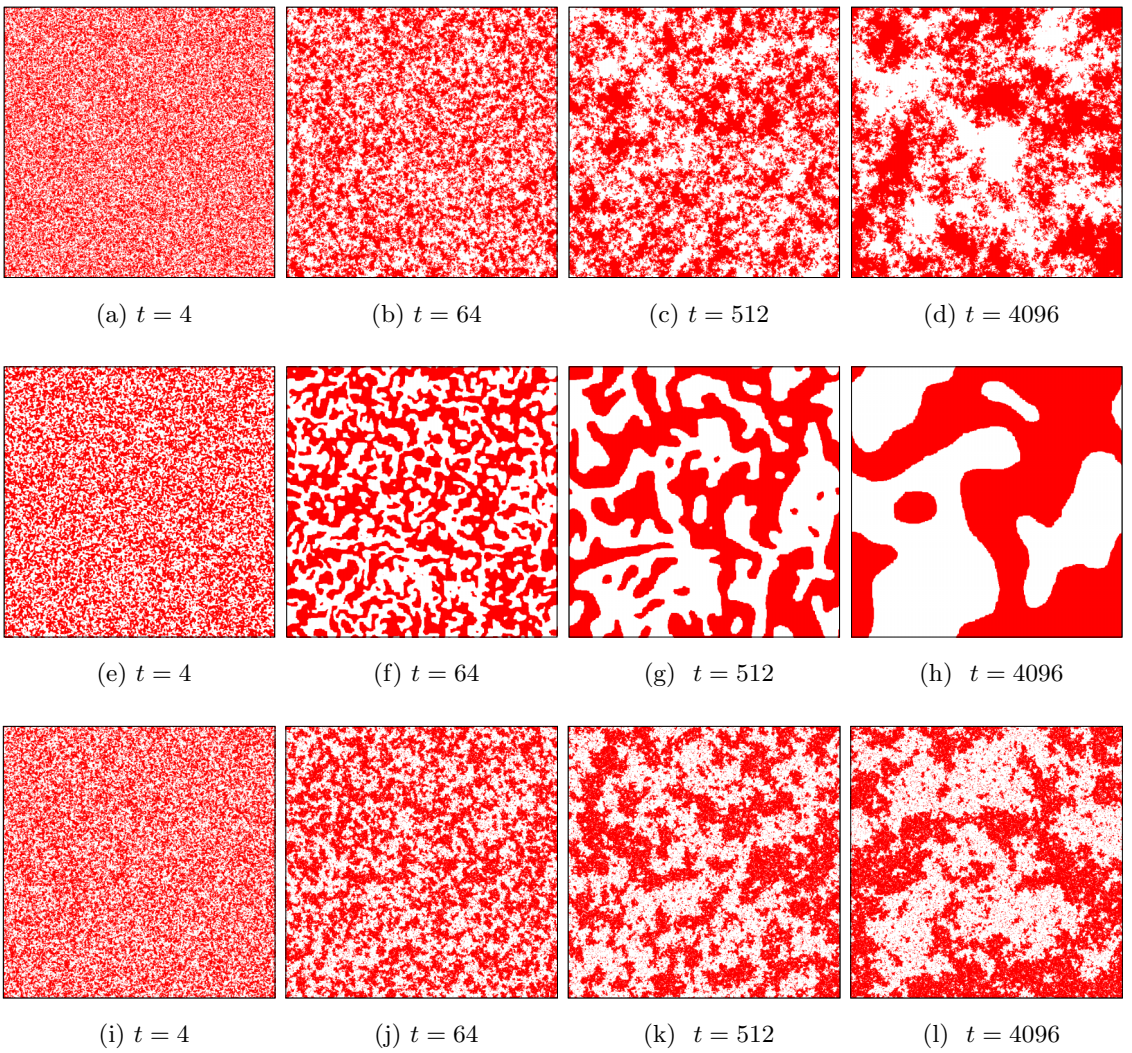

(a) $t = 4$ (b) $t = 64$ (c) $t = 512$ (d) $t = 4096$

(e) $t = 4$ (f) $t = 64$ (g) $t = 512$ (h) $t = 4096$

(i) $t = 4$ (j) $t = 64$ (k) $t = 512$ (l) $t = 4096$

FIG. 1. (Color online) Snapshots of the voter (first row) and Ising (second and third rows) models on a $2d$ square lattice with linear size $L = 640$ and periodic boundary conditions. The Ising model has been quenched to $T = 0$ (second row) and T_c (third row). The images were taken at the times indicated below the snapshots.

slowly in time we are able to analyze this dynamic regime in detail (contrary to the what happens in the Ising model, where $\ell_P(t)$ is such a fast-growing function of time that in practice critical percolation is reached too quickly to allow for a careful study of this dynamic regime).

The paper is organized as follows. In Sec. II we introduce the model and we summarize the time dependence of several observables that were derived analytically in the past for infinite-size systems. In Sec. III we present our numerical results. We discuss the violation of the scaling hypothesis as observed in the time dependence of the density of interfaces, persistence probability, two-time correlation function, and space-time correlation function of an infinite-size system. We then show our novel results on geometric properties of the largest cluster, number density of domain areas, and interface lengths in finite-size systems. We relate their properties to the fractal properties of these objects. More importantly, this analysis allows us to demonstrate the existence of the two dynamic regimes evoked in the previous paragraph: A first approach to critical site percolation and the further evolution towards complete consensus in a longer time scale. We end the paper with a concluding section.

II. ANALYTICAL RESULTS

The definition of the voter model is extremely simple. Each node i of a graph is endowed with a binary variable $s_i = \pm 1$. At each time step an agent i is selected at random along with one of its neighbors j and the selected agent takes the opinion of the neighbor, i.e., $s_i = s_j$. In the case of a voter model on a d-dimensional hypercubic lattice, the spin-flip rate for the site $\boldsymbol{x}$ is given by [25]

$$W_{\boldsymbol{x}}(s) = \frac{1}{2\tau}\left[1 - \frac{1}{2d}\, s_{\boldsymbol{x}}(t) \sum_{\boldsymbol{y}\in\mathcal{N}(\boldsymbol{x})} s_{\boldsymbol{y}}(t)\right], \qquad (2.1)$$

where $s = (s_{\boldsymbol{x}})_{\boldsymbol{x}\in\mathbb{Z}^d}$ denotes the state of the system at time t, $s_{\boldsymbol{x}}$ is the value of the spin on site $\boldsymbol{x}$, $\mathcal{N}(\boldsymbol{x})$ is the set of its neighboring sites, and τ defines the time scale of the process. This particular form of spin-flip rate, which is just a constant

times the fraction of disagreeing neighboring sites, defines the so-called linear voter model. It is possible to define other voterlike models in which the spin-flip rate is not simply a linear function of the local effective field $h_{\boldsymbol{x}} = \sum_{\boldsymbol{y}\in\mathcal{N}(\boldsymbol{x})} s_{\boldsymbol{y}}$ but still satisfy the Z_2 symmetry and have similar properties [1,26]. We will focus on the model with spin-flip rate (2.1) here. Note also that we are taking $\boldsymbol{x} \in \mathbb{Z}^d$. We will assume the lattice to be infinite in all the calculations appearing further in this section, though we will be especially concerned with finite-size effects in Sec. III.

Equation (2.1) implies that this spin model has no bulk noise, i.e., if a site "agrees" with all its nearest-neighbors, its spin-flip rate vanishes. In this sense, the dynamics are similar to the zero-temperature Glauber ones. The consequence is that the "consensus" states, i.e., the states in which all sites have the same opinion, are "absorbing" states. Indeed, if the system reaches one of the two consensus states, it will never leave it.

However, this does not mean that the asymptotic steady state must be one of full consensus. In fact, it turns out that the coarsening process is not always effective in bringing the system towards a single-domain state, and whether it does or not depends on the dimensionality of the lattice. For $d \leqslant 2$ the system coarsens until ultimately reaching a single domain state, while for $d > 2$ there is an infinite family of noncompletely ordered steady states [11,13]. The discrepancy in the asymptotic regime reached above and below $d = 2$ will be further discussed in this section.

The probability distribution satisfies the master equation

$$\frac{d}{dt}P(s,t) = \sum_{\boldsymbol{x}}[W_{\boldsymbol{x}}(s^{\boldsymbol{x}})P(s^{\boldsymbol{x}},t) - W_{\boldsymbol{x}}(s)P(s,t)], \qquad (2.2)$$

where $s^{\boldsymbol{x}}$ is the configuration that differs from s only in that the spin on the site $\boldsymbol{x}$ is reversed. One can then derive a set of differential equations for the n-spin time-dependent correlation functions $\langle s_{\boldsymbol{x_1}}...s_{\boldsymbol{x_n}}\rangle = \sum_s s_{\boldsymbol{x_1}}...s_{\boldsymbol{x_n}}P(s,t)$ and find that, since the update rule $W_{\boldsymbol{x}}$ is simply linear in the local spin, the equations for the correlation functions of different order decouple.

The single-body correlation function or average magnetization satisfies [8,27]

$$\frac{d}{dt}\langle s_{\boldsymbol{x}}\rangle = -2\langle s_{\boldsymbol{x}}W_{\boldsymbol{x}}(s)\rangle = \frac{1}{2\tau d}\Delta_{\boldsymbol{x}}\langle s_{\boldsymbol{x}}\rangle, \qquad (2.3)$$

where $\Delta_{\boldsymbol{x}}$ denotes the discrete Laplace operator,

$$\Delta_{\boldsymbol{x}}\langle s_{\boldsymbol{x}}\rangle \equiv -2d\langle s_{\boldsymbol{x}}\rangle + \sum_{i=1}^{d}(\langle s_{\boldsymbol{x}+\mathbf{e}_i}\rangle + \langle s_{\boldsymbol{x}-\mathbf{e}_i}\rangle), \qquad (2.4)$$

and $\{\mathbf{e}_i\}_{i=1,...,d}$ are the set of unit vectors defining the lattice. In the infinite-system-size limit or for periodic boundary conditions all sites satisfy this same equation. For finite-size systems with open boundary conditions the sites at the edges should be considered separately.

Similarly, for the two-body correlation function one has [8,27]

$$\begin{aligned}\frac{d}{dt}\langle s_{\boldsymbol{x}}s_{\boldsymbol{y}}\rangle &= -2\langle s_{\boldsymbol{x}}s_{\boldsymbol{y}}[W_{\boldsymbol{x}}(s) + W_{\boldsymbol{y}}(s)]\rangle \\ &= \frac{1}{2\tau d}(\Delta_{\boldsymbol{x}} + \Delta_{\boldsymbol{y}})\langle s_{\boldsymbol{x}}s_{\boldsymbol{y}}\rangle. \end{aligned} \qquad (2.5)$$

Interestingly enough, Eq. (2.2) is mathematically equivalent to the master equation for a continuous-time symmetric random walk on $\mathbb{Z}^d$ with jumping rate τ^{-1}. As a result, the mean magnetization per site, defined as $m(t) = \lim_{L\to\infty} L^{-d}\sum_{\boldsymbol{x}\in\{1,...,L\}^d}\langle s_{\boldsymbol{x}}(t)\rangle$, plays the role of the total probability for the walker and is thus a conserved quantity. The same result can be obtained by summing both sides of Eq. (2.3) over all lattice sites. Notice that while the magnetization of a specific system does change in a single update event, the average over all sites and over all trajectories of the dynamics is conserved.

Consider a finite system with an initial fraction ρ of voters in the $+1$ state and $1-\rho$ in the -1 state, so the initial magnetization density is $m_0 = 2\rho - 1$. Suppose that the system reaches consensus in which the state of magnetization $m = +1$ occurs with probability $p_{+1}(\rho)$ and the state with $m = -1$ with probability $1 - p_{+1}(\rho)$. Then, since $m_0 = m_\infty$, one has $2\rho - 1 = 2p_{+1}(\rho) - 1$, hence $p_{+1}(\rho) = \rho$.

Concerning again Eq. (2.3), by using the discrete Fourier transform of $\langle s_{\boldsymbol{x}}\rangle$, one can prove that its general solution on an infinite-size lattice has the form [8,27]

$$\langle s_{\boldsymbol{x}}(t)\rangle = e^{-\frac{t}{\tau}}\sum_{\boldsymbol{y}\in\mathbb{Z}^d}\sigma_{\boldsymbol{y}}\,\mathcal{J}_{\boldsymbol{x}-\boldsymbol{y}}\left(\frac{t}{\tau d}\right), \qquad (2.6)$$

where $\sigma_{\boldsymbol{y}} = \langle s_{\boldsymbol{y}}(t=0)\rangle$ and $\mathcal{J}_{\boldsymbol{x}}$ is a shorthand notation for the multi-index modified Bessel functions, $\mathcal{J}_{\boldsymbol{x}}(u) = \prod_{i=1}^{d}\mathcal{I}_{x_i}(u)$, with $\mathcal{I}_\alpha$ the usual modified Bessel function of order α.

If the initial configuration is such that a single $+1$ voter sits at the origin and is surrounded by a "sea" of undecided voters [i.e., $s_{\boldsymbol{x}}(0) = \pm 1$ with probability $1/2$ for all $\boldsymbol{x} \neq \mathbf{0}$] then, since $\sigma_{\boldsymbol{x}} = \delta_{\boldsymbol{x},\mathbf{0}}$, the solution to Eq. (2.3) reduces to $\langle s_{\boldsymbol{x}}(t)\rangle = e^{-t/\tau}\mathcal{J}_{\boldsymbol{x}}[t/(\tau d)]$. By using now the asymptotic relation $\mathcal{I}_\alpha(z) \sim e^z/\sqrt{2\pi z}$, $z \gg 1$, valid for any real α, one finds the asymptotic behavior of the average site magnetization, $\langle s_{\boldsymbol{x}}(t)\rangle \sim [2\pi t/(\tau d)]^{-d/2}$. Thus, a single voter relaxes to the average undecided opinion of the rest of the population.

The last result is exact but does not provide meaningful information on how the steady state of the system is reached. In this sense, a more interesting quantity is the two-body correlation function determined by Eq. (2.5). In order to solve this equation [8] one makes the assumption that at each time t the state of the system is translationally invariant, so $\langle s_{\boldsymbol{x}}s_{\boldsymbol{y}}\rangle$ depends on the lattice vectors $\boldsymbol{x}$ and $\boldsymbol{y}$ only through their difference $\boldsymbol{n} = \boldsymbol{x} - \boldsymbol{y}$. Then, by denoting $\mathrm{G}_{\boldsymbol{n}}(t) = \langle s_{\boldsymbol{x}}(t)s_{\boldsymbol{x}+\boldsymbol{n}}(t)\rangle$, Eq. (2.5) simplifies to

$$\frac{d}{dt}\mathrm{G}_{\boldsymbol{n}}(t) = \frac{1}{\tau d}\,\Delta_{\boldsymbol{n}}\mathrm{G}_{\boldsymbol{n}}(t), \qquad (2.7)$$

which should be solved subject to the boundary condition $\mathrm{G}_{\mathbf{0}}(t) = \langle s_{\boldsymbol{x}}^2(t)\rangle = 1$ for any t. In addition, it is natural to choose the initial condition $\mathrm{G}_{\boldsymbol{n}}(0) = \delta_{\boldsymbol{n},\mathbf{0}}$, which corresponds to a completely uncorrelated initial state. Equation (2.7) is basically identical to Eq. (2.3) apart from numerical factors, and one would be tempted to consider a solution of the form $\widetilde{\mathrm{G}}_{\boldsymbol{n}}(t) = \mathrm{e}^{-\frac{2t}{\tau}}\mathcal{J}_{\boldsymbol{n}}(2t/(\tau d))$. However, $\widetilde{\mathrm{G}}_{\mathbf{0}}(t)$ does not satisfy the boundary condition. In order to maintain $\mathrm{G}_{\mathbf{0}}(t) = 1$ throughout the evolution, one can reformulate the problem posed by Eq. (2.7) as the equivalent lattice diffusion problem with a constant localised source at the origin and look for a solution

of the form

$$\mathrm{G}_{\boldsymbol{n}}(t) = e^{-\frac{2t}{\tau}}\,\mathcal{J}_{\boldsymbol{n}}\left(\frac{2t}{\tau d}\right) + \int_0^t dt'\,S_d(t-t')\,e^{-\frac{2t'}{\tau}}\,\mathcal{J}_{\boldsymbol{n}}\left(\frac{2t'}{\tau d}\right) \tag{2.8}$$

with $S_d(t)$ the "strength" of the source. From a physical point of view, this solution corresponds to placing a source $\mathrm{G}_{\mathbf{0}}(t=0)$ at the initial time at the origin and supplement it by an additional input $S_d(t)dt$ that is added during the time interval $(t,t+dt)$ to keep the overall value unchanged. Equation (2.8) evaluated at the origin ($\boldsymbol{n}=\mathbf{0}$) becomes

$$1 = \left[e^{-\frac{2t}{\tau d}}\,\mathcal{I}_0\left(\frac{2t}{\tau d}\right)\right]^d + \int_0^t dt'\,S_d(t-t')\left[e^{-\frac{2t'}{\tau d}}\,\mathcal{I}_0\left(\frac{2t'}{\tau d}\right)\right]^d. \tag{2.9}$$

By using now the Laplace transform of the strength, $\hat{S}_d(\lambda) = \int_0^{+\infty} dt\,S_d(t)e^{-\lambda t}$, and the Laplace transform $\hat{T}_d(\lambda)$ of the function $T_d(t) = [\mathcal{I}_0(t)e^{-t}]^d$, one arrives at

$$\hat{S}_d(\lambda) = -1 + \frac{2}{\tau d}\left[\lambda\,\hat{T}_d\left(\frac{\tau d}{2}\lambda\right)\right]^{-1}. \tag{2.10}$$

Using now the integral representation of the modified Bessel function $\mathcal{I}_0$, namely $\mathcal{I}_0(x) = \frac{1}{2\pi}\int_0^{2\pi} dq\,e^{x\cos(q)}$, it is possible to express $\hat{T}_d$ in terms of the Watson integrals,

$$\hat{T}_d(\lambda) = \frac{1}{(2\pi)^d}\int_0^{2\pi}\cdots\int_0^{2\pi} dq_1\cdots dq_d\,\frac{1}{\lambda + d - \sum_{i=1}^d \cos q_i}, \tag{2.11}$$

and find an expression for $\hat{S}_d(\lambda)$. For example, in the case $d=1$, $\hat{S}_1(\lambda) = \sqrt{(\lambda+2)/\lambda}$. More complicated expressions arise when d is larger and ultimately there is no closed form for them. Nevertheless, we are just interested in the asymptotic behavior of the source strength S_d, which in turn is given by the low-λ limit of its Laplace transform [8],

$$\hat{S}_d(\lambda) \sim \begin{cases} \left(\frac{\tau}{2}\lambda\right)^{-\frac{1}{2}} & \text{if } d=1 \\ (\tau\lambda)^{-1}\ln^{-1}[1/(\tau\lambda)] & \text{if } d=2 \\ \left(\frac{\tau d}{2}\lambda\right)^{-1} & \text{if } d>2 \end{cases} \quad \text{as } \lambda\to 0 \tag{2.12}$$

and thus

$$S_d(t) \sim \begin{cases} \left(\frac{2t}{\tau}\right)^{-\frac{1}{2}} & \text{if } d=1 \\ \ln^{-1}\left(\frac{t}{\tau}\right) & \text{if } d=2 \\ \text{const.} & \text{if } d>2 \end{cases} \quad \text{as } t\to+\infty \tag{2.13}$$

In $d=2$, the long-time behavior of the source strength in the integral is $S_2(t-t') \simeq 1/\ln[(t-t')/\tau] \simeq 1/\ln(t/\tau)$. Using the asymptotic relations for $\mathcal{I}_\alpha$, and calling $\boldsymbol{n} = (n_1,n_2)$, Eq. (2.8) implies

$$\mathrm{G}_{\boldsymbol{n}}(t) \simeq \frac{1}{2\pi t} + \frac{c}{\ln(t/\tau)}\int_0^t dt'\,e^{-\frac{2t'}{\tau}}\,\mathcal{I}_{n_1}\left(\frac{t'}{\tau}\right)\mathcal{I}_{n_2}\left(\frac{t'}{\tau}\right) \tag{2.14}$$

as $t\to+\infty$ dropping corrections $\mathcal{O}(t^{-2})$, with c a numerical factor to be determined. Using the integral representation of the modified Bessel function $\mathcal{I}_n$ for integer values of n, that is, $\mathcal{I}_n(t) = (2\pi)^{-1}\int_{-\pi}^{\pi} dk\,\exp[t\cos k - i\,n\,k]$, Eq. (2.14) reduces to

$$\mathrm{G}_{\boldsymbol{n}}(t) \simeq \frac{c}{\ln(t/\tau)}\frac{1}{(2\pi)^2}\int_{-\pi}^{\pi} dk_1\int_{-\pi}^{\pi} dk_2\,\mathrm{e}^{-i\boldsymbol{n}\cdot\boldsymbol{k}}\,\hat{f}(\boldsymbol{k},t) + \mathcal{O}\left(\frac{1}{t}\right), \tag{2.15}$$

where $\boldsymbol{k} = (k_1,k_2)$ and the function $\hat{f}(\boldsymbol{k},t)$ is given by

$$\hat{f}(\boldsymbol{k},t) = \tau\,\frac{1-e^{-\frac{t}{\tau}(2-\cos k_1-\cos k_2)}}{2-\cos k_1-\cos k_2}. \tag{2.16}$$

Apart from a time-dependent prefactor, one can recognize in $\hat{f}$ the dynamical structure factor of the system, which is defined as the lattice Fourier transform of the space-time-dependent correlation function,

$$S(\boldsymbol{k},t) = \frac{1}{\ln(t/\tau)}\,\hat{f}(\boldsymbol{k},t) \;\propto\; \sum_{\boldsymbol{n}\in\mathbb{Z}^2}\mathrm{G}_{\boldsymbol{n}}(t)\,\mathrm{e}^{i\boldsymbol{n}\cdot\boldsymbol{k}}. \tag{2.17}$$

In the limit $|\boldsymbol{k}|\to 0$, $\hat{f}$ can be approximated as $\hat{f}(\boldsymbol{k},t) \simeq 2\,\tau\,k^{-2}(1-e^{-\frac{t}{2\tau}k^2})$, where $k=|\boldsymbol{k}|$, i.e., it becomes isotropic in k space. Then the large-distance behavior of the correlation function is characterized by the scaling form

$$\mathrm{G}_{\boldsymbol{n}}(t) \;\sim\; \frac{1}{\ln(t/\tau)}\,f\left(\frac{|\boldsymbol{n}|}{\sqrt{t/2\tau}}\right), \tag{2.18}$$

where the scaling function f is just given by the inverse Fourier transform of $\hat{f}$. Equation (2.18) clearly displays the emergence of a dynamical characteristic length $\ell(t)$ which scales as $\sqrt{t}$ and the logarithmic violation of dynamic scaling.

An interesting quantity that can be extracted from the two-body correlation function is the density of reactive interfaces ρ, defined as the average value of the fraction of unsatisfied bonds or, equivalently, the fraction of neighboring voters with disagreeing opinions. This quantity is linked to the correlation function through the relation

$$\rho(t) = \frac{1}{2}\left\{1 - \frac{1}{2d}\sum_{i=1}^{d}\left[\mathrm{G}_{\mathbf{e}_i}(t) + \mathrm{G}_{-\mathbf{e}_i}(t)\right]\right\} = \frac{1}{2}[1-\mathrm{G}_{\mathbf{e}}(t)], \tag{2.19}$$

where $\mathbf{e}_i$ are the lattice unit vectors. Note that the sum over the nearest-neighbors can be lifted since the dynamics is isotropic along the d principal directions of the lattice. From Eq. (2.8) evaluated at $\boldsymbol{n} = (1,0,\ldots,0)$ and the fact that $\mathrm{G}_{\mathbf{0}} \equiv 1$, one obtains

$$\rho(t) = \frac{1}{2}\,e^{-\frac{2t}{\tau}}\,\mathcal{I}_0^{d-1}\left(\frac{2t}{\tau d}\right)\left[\mathcal{I}_0\left(\frac{2t}{\tau d}\right) - \mathcal{I}_1\left(\frac{2t}{\tau d}\right)\right] + \frac{1}{2}\int_0^t du\,S_d(t-u)\,e^{-\frac{2u}{\tau}}\,\mathcal{I}_0^{d-1}\left(\frac{2u}{\tau d}\right) \times\left[\mathcal{I}_0\left(\frac{2u}{\tau d}\right) - \mathcal{I}_1\left(\frac{2u}{\tau d}\right)\right]. \tag{2.20}$$

Combining the latter equation with Eqs. (2.13) and the asymptotic relations $\mathcal{I}_0(z) \simeq \mathcal{I}_1(z) \simeq e^z[1/\sqrt{2\pi z} + \mathcal{O}(z^{-3/2})]$ and $\mathcal{I}_0(z) - \mathcal{I}_1(z) \simeq e^z[1/\sqrt{8\pi z^3} + \mathcal{O}(z^{-5/2})]$, the asymptotic behavior of the density of reactive interfaces is found to

be [8,12]

$$\rho(t) \sim \begin{cases} t^{-\frac{1}{2}} & \text{if } d=1 \\ \ln^{-1}(t/\tau) & \text{if } d=2 \\ a - bt^{-d/2} & \text{if } d>2 \end{cases} \quad \text{as } t \to +\infty. \tag{2.21}$$

These results allow us to establish some conclusions on the coarsening process in the voter model: In $d \leqslant 2$ the probability that two voters at a given separation had opposite opinion vanishes asymptotically, no matter how much distant they are, and coarsening eventually leads to a single-domain final state. In $d > 2$, an infinite system reaches a dynamic frustrated state, where opposite-opinion voters coexist and continually evolve in such a way that the average concentration of each type of voters remains fixed. Dimension $d = 2$ is particular since it lies at the border between the two cases. There is a coarsening process which brings the system towards the single-domain state, but it is very slow, since the density of active interfaces vanishes only as $1/\ln(t/\tau)$.

As a last effort, we derive the two-time correlation function, defined as $A_{\boldsymbol{x}}(t,t_0) = \langle s_{\boldsymbol{x}}(t) s_{\boldsymbol{x}}(t_0)\rangle$, which is an interesting quantity to look at since it provides information on the typical time scale for the process to reach a steady state. For fixed t_0 and $\boldsymbol{x_0} \in \mathbb{Z}^d$, let us introduce the function $F_{\boldsymbol{x}}(t;\boldsymbol{x_0},t_0) = \langle s_{\boldsymbol{x}}(t+t_0) s_{\boldsymbol{x_0}}(t_0)\rangle$ for any $\boldsymbol{x} \in \mathbb{Z}^d$ and $t \geqslant 0$. Dropping for a moment the dependence of F on t_0 and $\boldsymbol{x_0}$, it is easy to see that it satisfies the same equation as the single-body correlation function, i.e., $\frac{d}{dt} F_{\boldsymbol{x}}(t) = \frac{1}{2\tau d} \Delta_{\boldsymbol{x}} F_{\boldsymbol{x}}(t)$, apart from a factor $1/2$. Thus $F_{\boldsymbol{x}}(t) = e^{-t/\tau} \sum_{\boldsymbol{y}} f_{\boldsymbol{y}} \mathcal{J}_{\boldsymbol{x}-\boldsymbol{y}}(t/\tau d)$, where $f_{\boldsymbol{y}}(\boldsymbol{x_0},t_0) = \langle s_{\boldsymbol{y}}(t_0) s_{\boldsymbol{x_0}}(t_0)\rangle$. Then, assuming that at each time the state of the system is spatially translational invariant and using $A_{\boldsymbol{x}}(t,t_0) = F_{\boldsymbol{x}}(t-t_0;\boldsymbol{x},t_0)$, one gets

$$A_{\boldsymbol{x}}(t,t_0) = e^{-(t-t_0)/\tau} \sum_{\boldsymbol{n}\in\mathbb{Z}^d} \mathrm{G}_{\boldsymbol{n}}(t_0)\, \mathcal{J}_{\boldsymbol{n}}\left(\frac{t-t_0}{\tau d}\right), \tag{2.22}$$

with the dependence on $\boldsymbol{x}$ disappearing consistently with the hypothesis of translational invariance. As a simple check we verify that setting $t = t_0$ in Eq. (2.22) we find $\mathrm{G}_{\boldsymbol{0}}(t_0)$. Indeed, using $\mathcal{J}_{\boldsymbol{n}}(0) = \prod_{i=1}^d \mathcal{I}_{x_i}(0) = 0$ for all $\boldsymbol{n} \neq \boldsymbol{0}$ and $\mathcal{J}_{\boldsymbol{0}}(0) = \prod_{i=1}^d \mathcal{I}_{x_i=0}(0) = 1$ this fact is verified.

In the particular case $t_0 = 0$, if the initial configuration is completely uncorrelated, i.e., $\mathrm{G}_{\boldsymbol{n}}(0) = \delta_{\boldsymbol{n},\boldsymbol{0}}$, then the solution reduces to

$$A_0(t) = A(t,t_0=0) = e^{-t/\tau}\left[\mathcal{I}_0\left(\frac{t}{\tau d}\right)\right]^d \tag{2.23}$$

with asymptotic behavior $A_0(t) \sim [2\pi t/(\tau d)]^{-d/2}$.

In the limit $t \gg t_0$ one can use the asymptotic expansion of $\mathcal{J}_{\boldsymbol{n}}(u) = \prod_{i=1}^d \mathcal{I}_{x_i}(u) \simeq [e^u/\sqrt{2\pi u}]^d$ with $u = (t-t_0)/(\tau d)$ and, therefore,

$$\lim_{t\gg t_0} A_{\boldsymbol{x}}(t,t_0) = [2\pi(t-t_0)/(\tau d)]^{-d/2} \sum_{\boldsymbol{n}\in\mathbb{Z}^d} \mathrm{G}_{\boldsymbol{n}}(t_0). \tag{2.24}$$

The t_0-dependent last factor can be estimated as follows:

$$K(t_0) \equiv \sum_{\boldsymbol{n}\in\mathbb{Z}^d} \mathrm{G}_{\boldsymbol{n}}(t_0) \mapsto \int d^d x\, C(\boldsymbol{x},t_0) = 2\pi \int dr\, r\, C(r,t_0) \tag{2.25}$$

with $C(\boldsymbol{x},t)$ the space-time correlation function in the continuum space limit. Setting $d = 2$ and using the scaling function for $C(r,t_0)$ expressed in Eq. (2.18),

$$K(t_0) = 2\pi \int dr\, \frac{r}{\ln(t_0/\tau)}\, f\left(\frac{r}{\sqrt{t_0/\tau}}\right) \propto \frac{2\pi}{\ln(t_0/\tau)}\, \frac{t_0}{\tau}. \tag{2.26}$$

Going back to Eq. (2.24), this implies

$$\lim_{t\gg t_0} A_{\boldsymbol{x}}(t,t_0) \propto \frac{1}{\ln(t_0/\tau)}\ (t/t_0 - 1)^{-1}. \tag{2.27}$$

Further details on how to obtain the analytical results sketched in this section can be found in Refs. [8,12,27,28].

We have already explained how the asymptotic behavior of the space-time dependent correlation functions can be obtained in a way that exploits the special properties of the master equation. An alternative treatment of the many-body correlation functions uses an equivalence between the voter model and an auxiliary process of annihilating random walks [11,13,29]. By using this approach, Scheucher and Spohn obtained the same result for the dynamical structure factor in the small k and long-time limits for $d = 2$,

$$S(\boldsymbol{k},t) \sim \frac{1}{\ln(t/\tau)}\, \frac{1}{\kappa^2(t/\tau)}\, F\left[\frac{|\boldsymbol{k}|}{\kappa(t/\tau)}\right] \tag{2.28}$$

with $\kappa(t) \propto t^{-\frac{1}{2}}$ and $F(u) = \frac{1}{2u^2}(1 - e^{-u^2})$, as found by employing the master equation formalism. From here one recovers the asymptotic form for $C(\boldsymbol{x},t)$ in Eq. (2.18).

III. NUMERICAL ANALYSIS

In this section we present our numerical results. We first compare them to the analytical ones recalled in Sec. II for infinite-size systems and we later focus our attention on finite-size effects.

We define the model on a square lattice with linear size L and periodic boundary conditions. In all cases we start the dynamics at time $t = 0$ with a random initial condition with $s_{\boldsymbol{x}} = \pm 1$ with probability a half.

One unit of time (i.e., τ) corresponds to L^2 spin-flip attempts. As the system coarsens the number of flippable spins decreases and more attempts are necessary to change the configuration significantly. In order to accelerate the simulations we used a continuous-time Monte Carlo algorithm with the voter model dynamic rule. Unless otherwise stated, the quantities that we present below were averaged over 10^5 samples.

As we will be particularly concerned with the geometric properties of the coarsening process, let us give here a number of definitions that we will use in the rest of this section. We define a cluster or geometric domain as the ensemble of first-neighbor parallel spins. The cluster area is the number of spins belonging to it. Any such domain is surrounded by an interface that corresponds to the ensemble of broken first-neighbor links surrounding the cluster. The total interface length (external plus internal) is the number of such oppositely oriented spin pairs.

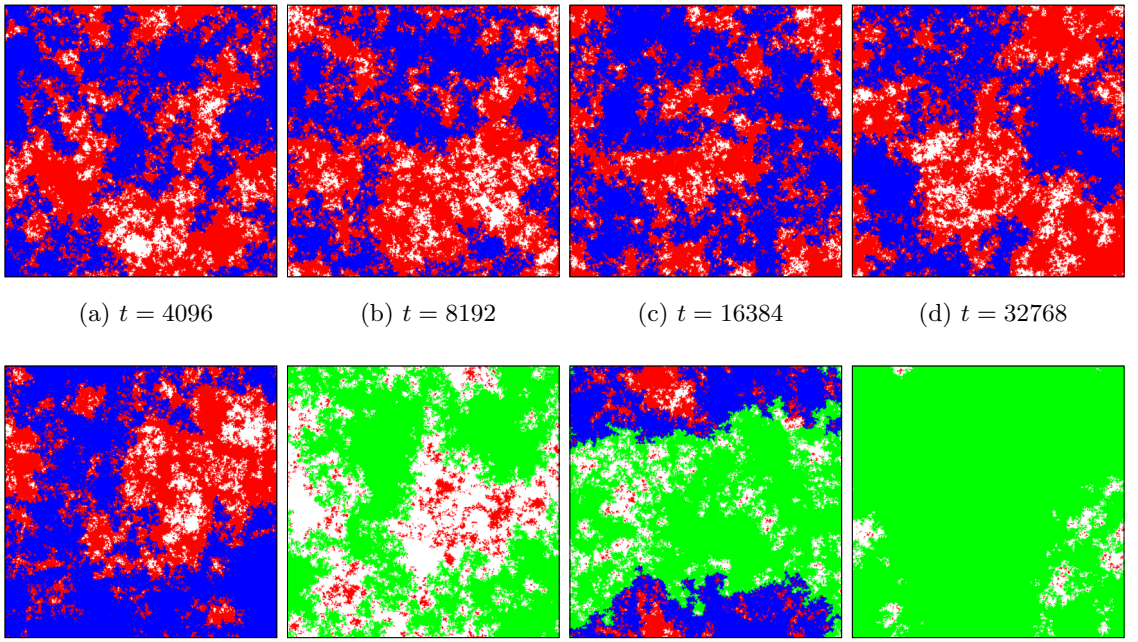

(a) $t = 4096$ (b) $t = 8192$ (c) $t = 16384$ (d) $t = 32768$

(e) $t = 65536$ (f) $t = 131072$ (g) $t = 262144$ (h) $t = 524288$

FIG. 2. (Color online) Snapshots of the voter model with linear size $L = 640$ and periodic boundary conditions. The times shown are $t_i = 2^i$, with $i = 12$–19. With the same convention as in Fig. 1, the $+1$ voters are in medium gray (red), while the -1 voters are in white. We highlight here the percolating clusters with different colors. Percolating clusters of $+1$ opinion are clear gray (green) and of -1 opinion are black (blue). A single domain of "$+1$" voters was reached at $t \approx 6.7 \times 10^5$.

A. Snapshots

In Fig. 1 we show three series of snapshots of the bidimensional voter model (first row) and the ferromagnetic Ising model at times $t = 4$, 64, 512, 4096 (henceforth all numerical times are expressed in MCs and we omit this time unit to lighten the notation). The Ising model (IM) has been quenched to zero temperature (second row) and the critical point (third row) and it evolves with a heat-bath Monte Carlo algorithm. Red and white points represent the two spin configurations. The snapshots illustrate the coarsening phenomenon induced by the different microscopic dynamics. In the case of the $2d$IM instantaneously quenched to $T = 0$ the dynamics are purely curvature driven: for sufficiently long times, all the interfaces move with a local velocity that is proportional to the local curvature [14,15]. As a result, the interfaces tend to disappear independently of one another, i.e., there are no coalescence processes. Instead, in the voter model the dynamics are driven by interfacial noise. In other words, if the initial configuration consisted of a single flat interface between two domains of opposite opinion, opinions would slowly diffuse from one domain into the other and, after a sufficiently long time, the original sharp wall would become a diffuse interface. As one can see from the snapshots, phase ordering still occurs but the resulting domains are very jagged and preserve their fractal geometry even at the late stages of evolution. Note, however, that the dynamics of the zero temperature Ising model and the voter model have one important feature in common, namely, they are both characterized by the absence of bulk fluctuations. But they also show one important difference in the morphological properties of their interfaces. Indeed, the domain walls in the voter model are more similar to the ones in the critically quenched Ising model, shown in the third series of snapshots in the same figure, than to the ones in the Ising model evolving at any subcritical temperature. The critical configurations are, though, plagued with bulk fluctuations, and these are absent in the voter model.

In Fig. 2 we display a series of snapshots of the voter model for even longer times than the ones used in Fig. 1 highlighting the percolating clusters of the two types. These configurations could be compared to the ones shown in Ref. [24] for the $2d$IM quenched to $T = 0$. We note that the identity and form of the percolating clusters are not preserved in the first seven snapshots, until the system enters the late stage of evolution and finds full consensus.

In Sec. III F we identify the largest cluster in the system and we study several of its properties letting us obtain in this way the exponent linking the system size to the time needed to reach percolation, and the fractal dimension of the percolating cluster and the one of its perimeter.

In the case of a finite lattice with periodic boundary conditions one can distinguish two types of domains: the ones that are homotopic to a point on the torus and the ones that wrap around the hole and cannot be completely shrunk without breaking into disconnected pieces. Even though the former can have a linear size comparable or even bigger than the one of the system, we identify the percolating clusters as the ones that wrap around the torus hole only.

B. Interface density

In Sec. II we provided an expression for the long-time behavior of the fraction of active interfaces. In the disordered initial condition $\rho(0) \simeq 1/2$. In $d = 1$ the voter model is

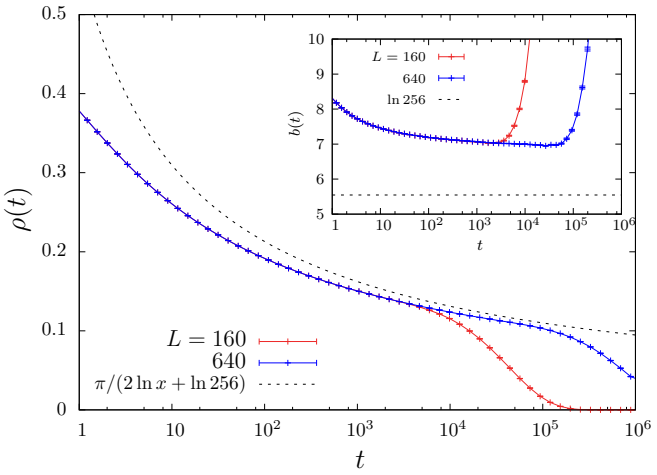

FIG. 3. (Color online) Concentration of active interfaces $\rho(t) = [1 - \langle s_{\boldsymbol{x}}(t) s_{\boldsymbol{x}+\mathbf{e}_i}(t)\rangle]/2$ as a function of time. Data for $L = 160$ and 640 are presented in a log-linear form. The error bars are smaller than the symbol sizes. The dotted (black) line represents the analytic asymptotic form $\rho(t) = a/(2\ln t + b)$ with $a = 3.14$ and $b = 5.54$. In the inset we show $b = \pi/\rho(t) - 2\ln t$ as a function of t for different lattice sizes together with the analytic value 5.54 shown with a horizontal dashed line. See the main text for a discussion.

equivalent to the Glauber IM and $\rho(t)$ decays as $t^{-1/2}$ while in $d > 2$ the density of interfaces converges to a constant, $\rho(t) \sim a - bt^{-d/2}$. In $d = 3$ the model has, then, blocked configurations asymptotically, as in the $2d$ and $3d$ IM at $T=0$ [30,31]. In the case of $d = 2$, $\rho(t)$ decays logarithmically and several authors [32,33] tried to study this particular behavior with Monte Carlo simulations. By starting from Eq. (2.20) it is possible to obtain a more refined estimate of $\rho(t)$ [8],

$$\rho(t) = \frac{\pi}{2\ln t + \ln 256} + O\left(\frac{\ln t}{t}\right). \tag{3.1}$$

This result has to be contrasted to the algebraic decay, $\rho(t) \sim t^{-d/z_d}$, of curvature-driven domain growth. For instance, in the $2d$IM model this same quantity decays as $\rho(t) \simeq \ell(t)^{-d} = t^{-d/z_d} = t^{-1}$, with $\ell(t)$ the characteristic growing length and $z_d = 2$.

In Fig. 3 we present numerical data for $\rho(t)$ in a voter model with linear size $L = 160$ and 640 with times reaching $t = 10^6$. The analytic result in the asymptotic limit $f(t) = a/(2\ln t + b)$ with $a = \pi$ and $b = \ln 256 \simeq 5.54$ accompanies the data as a dotted (black) line. We have performed detailed fits of the data finding that the parameter a approaches the analytic value quickly. We then fixed $a = \pi$ and we measured the parameter b by studying $b = \pi/\rho(t) - 2\ln t$ as a function of t for different system sizes [$\rho(t)$ are the measured values]. We show the result of this analysis in the inset to the same figure. The approach to the analytic value shown as a black dotted horizontal line is indeed very slow. This fact explains why several authors did not see the asymptotic law in their numerical data and used instead a different logarithmic form, $\rho(t) = C\ln^{-\sigma} t$, with an effective exponent $\sigma \approx 0.6$, to fit their data [8,33,34].

C. Consensus time

With much longer simulations we were able to measure the average consensus time, $\langle \mathcal{T}\rangle = N_s^{-1}\sum_{i=1}^{N_s} \mathcal{T}_i$ with $\mathcal{T}_i$ the time required by the i-th sample to reach full alignment and N_s the total number of samples. In Fig. 4(a) we show the results obtained by averaging over at least 7×10^3 realisations of the dynamics for each value of the lattice size L. The averaged consensus time approximately follows the law $\langle \mathcal{T}\rangle(L) \sim L^2$.

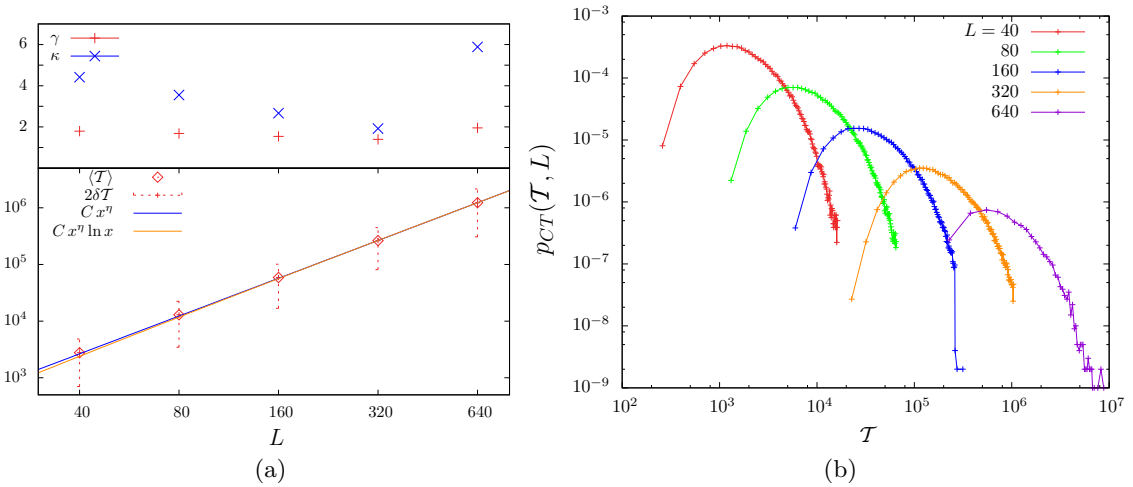

FIG. 4. (Color online) (a) The average consensus time $\langle \mathcal{T}\rangle$ (red diamonds) for different values of the lattice linear size L in a log-log plot. The value of $\langle \mathcal{T}\rangle$ has been computed over approximately 10^5 samples for the smaller sizes and over about 7×10^3 samples for $L = 640$. We report also the approximate width of the distribution, computed as the standard deviation of the data collected, $\delta\mathcal{T} = [N_s^{-1}\sum_{i=1}^{N_s}(t_i - \langle \mathcal{T}\rangle)^2]^{1/2}$, as vertical dashes with length $2\delta\mathcal{T}$ on each data point. Roughly, $\delta\mathcal{T}/\langle \mathcal{T}\rangle \simeq 0.74$ for all the sizes. The function $C\,x^\eta$ was fitted to the few data points available, yielding $\eta \simeq 2.21$ and $C \simeq 0.75$. By introducing a logarithmic prefactor, $C\,x^\eta \ln x$, the fit yields instead $\eta \simeq 2.05$ and $C \simeq 0.33$. In the upper part of the same panel we report the skewness γ and the kurtosis κ of the sampled distributions in order to quantify the deviations from a Gaussian form. (b) The distribution of consensus times for different system sizes L given in the key.

However, in Sec. II we recalled that the correlation functions suffer from logarithmic correction. Therefore, we tried to take into account this kind of correction by fitting the function $C\,L^{\eta}\ln L$ to the data $(L,\langle\mathcal{T}\rangle(L))$ and we obtained $\eta = 2.05 \pm 0.01$, $C = 0.33 \pm 0.02$, and a better agreement with the numerical data than with the pure power law.

An estimate of the characteristic width of the probability distribution of the consensus time is given by the standard deviation, $\delta\mathcal{T} = [N_s^{-1} \sum_{i=1}^{N_s} (\mathcal{T}_i - \langle\mathcal{T}\rangle)^2]^{1/2}$. The relative standard deviation $\delta\mathcal{T}/\langle\mathcal{T}\rangle$ was found to lie in the interval 0.70–0.75 for every L and no particular dependence on the number of samples was observed for $N_s > 10^3$. To highlight this behavior we added vertical dashes of width $2\delta\mathcal{T}(L)$ centered on each one of the data points in Fig. 4(a). We stress that these dashes do not represent any type of error on the numerical value of the average consensus time but only a measure of the average dispersion of our data on the available population of samples.

In Fig. 4(b) we show the histogram of consensus times $p_{\rm CT}(\mathcal{T},L)$ for the different lattice sizes that have been simulated. The curves have approximately all the same shape when plotted in a log-log scale, so it is reasonable to assume the following scaling ansatz:

$$p_{\rm CT}(\mathcal{T},L) = L^{-\alpha}\,\mathcal{P}\left(\frac{\mathcal{T}}{L^{\beta}\,\ln L}\right) \tag{3.2}$$

with exponents α and β to be determined. Equation (3.2) simply states that the probability distributions of the consensus time for finite systems with different size have identical form, apart from a prefactor, if time is rescaled by a typical time $\mathcal{T}_{\rm typ} \sim L^{\beta}\ln L$. This is a natural choice since $\langle\mathcal{T}\rangle \sim L^2 \ln L$ and thus we expect β to be very close to 2. In Fig. 5 we show the result of the scaling for $\beta = 2$ and $\alpha = 2.22$. We could not appreciate significant improvements of the collapse for values of β that differ slightly from 2, so our assumption was confirmed.

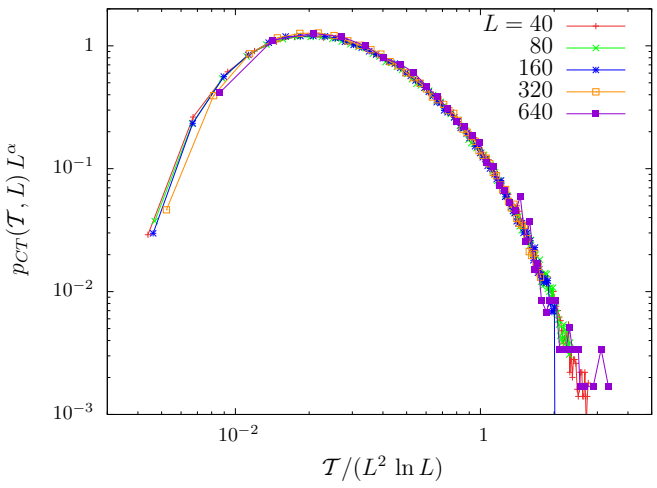

FIG. 5. (Color online) Rescaled histogram of the consensus time $p_{\rm CT}(\mathcal{T},L)$ for different lattice sizes. Time $\mathcal{T}$ is rescaled by $L^2 \ln L$, while the value of $p_{\rm CT}(\mathcal{T},L)$ is multiplied by L^{α}. The best collapse of the different curves was obtained for $\alpha \simeq 2.22$.

The upper part of Fig. 4(a) displays the skewness, $\gamma \equiv N_S^{-1} \sum_{i=1}^{N_s} (\mathcal{T}_i - \langle\mathcal{T}\rangle)^3/\delta\mathcal{T}^3$, and kurtosis, $\kappa \equiv N_S^{-1} \sum_{i=1}^{N_s} (\mathcal{T}_i - \langle\mathcal{T}\rangle)^4/\delta\mathcal{T}^4 - 3$, of $p_{\rm CT}(\mathcal{T},L)$ as a function of system size. The deviation from zero of the former quantifies the asymmetry of $p_{\rm CT}$ and of the latter gives a further idea of the non-Gaussian character of the distribution. The skewness seems to have converged to a system-size-independent value that is slightly higher than 1, while the kurtosis still varyies significantly for different system sizes. The last data points, for $L = 640$, are clearly not converged and many more samples would be needed to reach a good estimate for them.

D. Persistence and autocorrelation

In general one defines $P_n(t)$ as the probability distribution for the number of opinion changes n experienced by a voter during the time interval $(0,t)$, with $n \in \{0,1,2,\dots\}$ [27]. The first of these quantities, $P_0(t)$, is equal to the fraction of voters who did not change opinion up to time t, i.e., the persistence probability [35]. In terms of spins, it measures the fraction of sites that have not experienced any spin-flip up to time t. In most statistical physics models [35], the persistence decays in time with a power law $t^{-\theta}$ with a new independent persistence exponent θ. In the two-dimensional Glauber-Ising model at zero temperature, the exponent θ has been evaluated numerically with high precision and it takes the value $\theta \approx 0.199(2)$ for initial conditions with short-range correlations [36]. The asymptotic behavior of P_0 in the voter model in $d \geqslant 2$ was first found numerically [27] and then computed analytically with a mapping onto a continuum reaction-diffusion process and the use of field theoretical tools [37]. In $d = 2$,

$$P_0(t) \sim k\,\exp[-a\ln^2 t + \mathcal{O}(\ln t)] \tag{3.3}$$

for our choice $\tau d = 2$. The difference in the behavior of the persistence between the $2d$IM and the $2d$ voter model was investigated by Drouffe and Godrèche [26], who introduced a class of stochastic processes on a $2d$ square lattice that interpolate between these two. They also confirmed the unusual time dependence of the persistence decay in the $2d$ voter model with numerical simulations.

In this context, we tried to recover the theoretical prediction in Eq. (3.3) with simulations of the voter model with different sizes. We present data for $L = 160$ and $L = 640$ in Fig. 6(a). By fitting the simulation data to the function in Eq. (3.3) we found $a \approx 0.26$ and $k \approx e^{0.36} \simeq 1.44$. The estimated value of a is quite close to the theoretical value predicted by Howard and Godrèche [37], who found $a \simeq 1/4$ with corrections of order 0.01.

In Sec. II we showed that the autocorrelation with a completely uncorrelated initial configuration, $A_0(t)$, has the asymptotic behavior $A_0(t) \simeq (\pi t)^{-1}$ in $d = 2$, with the choice $\tau = 1$. In Fig. 6 we show numerical data for $A_0(t)$ in a system with linear size $L = 640$. As one can see, the data are in good agreement with the theoretical prediction.

In Fig. 7 we plot, instead, the two-time autocorrelation function $A(t,t_0)$ for values of $t_0 > 0$, and two different lattice sizes. At sufficiently long waiting-time t_0 the curves tend to flatten, losing their decay. This is clearer in the left panel where data for the smaller size, $L = 160$, are shown. In this case,

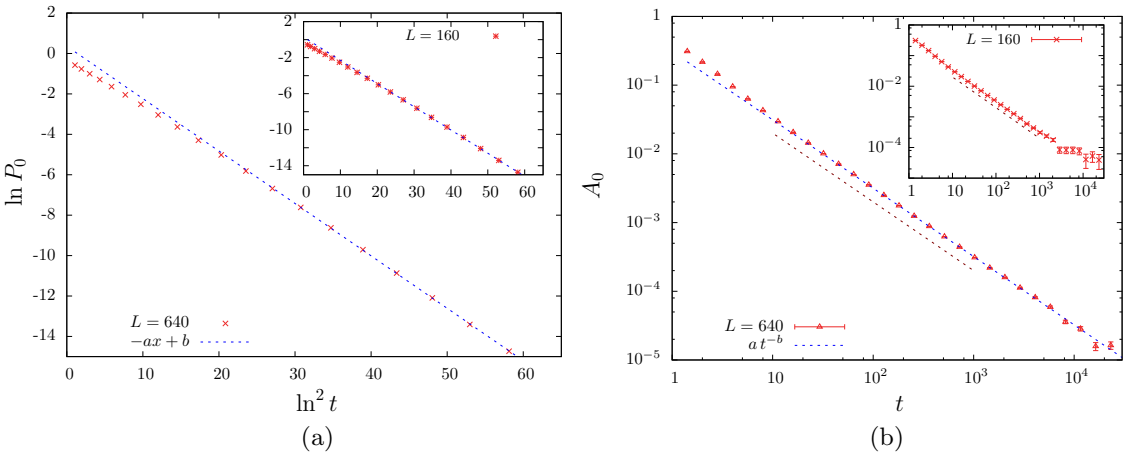

FIG. 6. (Color online) (a) The logarithm of the persistence probability, $\ln P_0$, against $\ln^2 t$, for a system of size $L = 640$. A linear fit to the data in this scale, $f(x) = b - ax$, gives $a \simeq 0.26$ and $b \simeq 0.36$ (the fitting curve is showed as a dashed blue line). The persistence has been calculated as an average over 5×10^4 realizations of the dynamics. Data for $L = 160$ are shown in the inset along with their fitting curve. (b) Time dependence of the autocorrelation with the initial configuration, A_0, in a double logarithmic scale. The function $f(t) = at^{-b}$ has been fitted to the numerical data, yielding $b = 0.995$ and $a = 0.308$, which are both in agreement with what theory predicts, i.e., $A(t) \sim (\pi t)^{-1}$, shown with a dark dashed segment. In the inset we show data for $L = 160$ analyzed in a similar fashion.

all curves reach a plateau for $t - t_0 \gtrsim 10^4$, signaling that the steady state has been reached. Indeed, we have calculated the average consensus time for a system with size $L = 160$ (see Fig. 4), and we found $\mathcal{T}_{160} \simeq 6 \times 10^4$, which is compatible with the behavior of the autocorrelation function. The same feature is expected to arise for the larger size $L = 640$ at a still longer time delay. In the case $L = 640$ we scaled the data to the analytic form (2.27) by plotting $\ln t_0\ A(t,t_0)$ against $t/t_0 - 1$ in Fig. 8. The scaling is very good for $t_0 \geqslant 256$.

The numerical analysis of several averaged correlation functions that we have presented so far is in good agreement with the theoretical predictions for infinite-size systems recalled in Sec. II. However, we will see in the following part of this section that by studying other geometrical observables, we get access to aspects of the dynamics that remain hidden in the correlation functions. This analysis will allow us to uncover another dynamic regime.

E. Averaged number of wrapping clusters

We analyzed the time dependence of the average number of wrapping domains per sample, $N_P(t; L)$, by supposing that it only depends upon a scaling variable,

$$N_P(t; L) = \mathcal{N}\left(\frac{t}{L^{\alpha_P}}\right), \tag{3.4}$$

with α_P a parameter to be determined and $\mathcal{N}(u)$ a scaling function. At strictly zero argument $\mathcal{N}(0) = 0$ since the initial random configuration is below the critical percolation threshold. At infinite value of the argument $\mathcal{N}(\infty) \to 1$ since the final state of full consensus has a single domain. In order to estimate α_P we tried to collapse $N_P(t; L)$ for different values of L by plotting it against the rescaled time t/L^{α_P} with trial values of α_P. The values of α_P that gave the best collapse were found in the range 1.65–1.68, and in Fig. 9 we present the

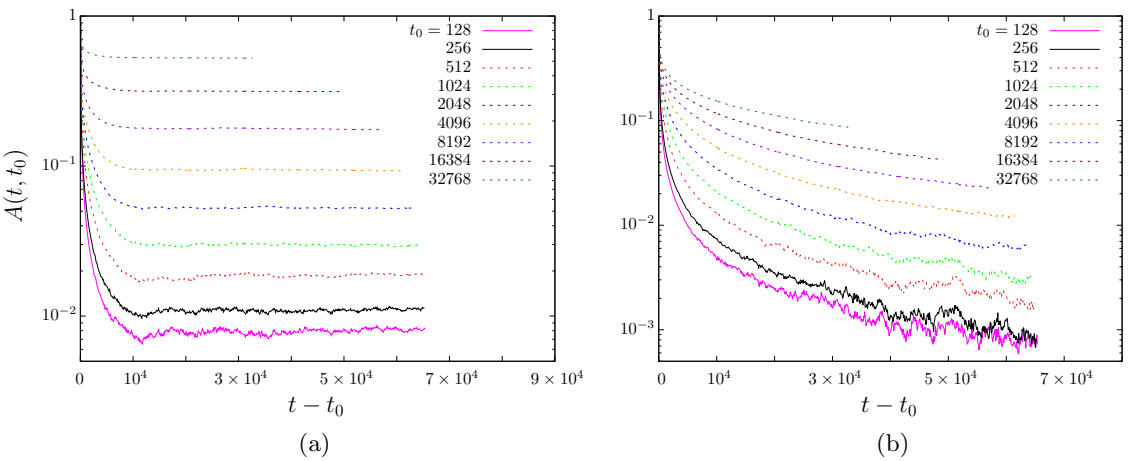

FIG. 7. (Color online) The two-time autocorrelation function $A(t,t_0)$ against time-delay $t - t_0$ for different values of the waiting-time t_0. Panels (a) and (b) show data for systems with linear size $L = 160$ and $L = 640$, respectively.

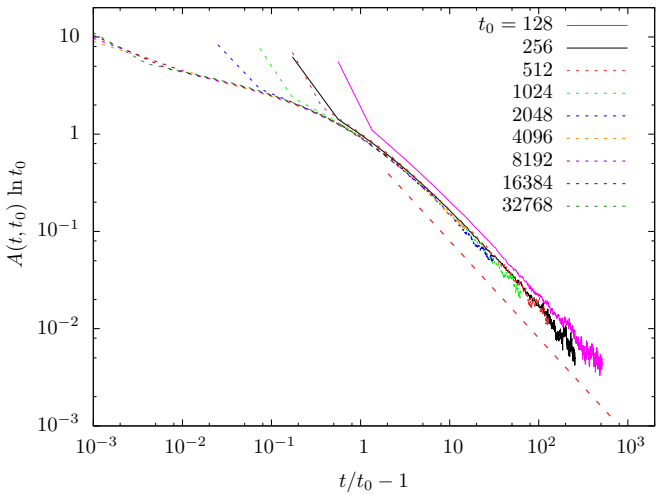

FIG. 8. (Color online) The two-time correlation function $A(t,t_0)$ times $\ln t_0$ against $(t/t_0 - 1)$, for different values of the waiting time t_0, in a log-log scale. A segment with slope -1 is shown as a guide-to-the-eye to stress the good agreement with the exponent found analytically.

case

$$\alpha_P = 1.667. \tag{3.5}$$

Even though the quality of the collapse for $t/L^{\alpha_P} < 0.1$ is very good, we must point out that this is a quite rough estimate, since we could not appreciate remarkable differences between slightly different values of α_P in the aforementioned interval. Deviations from the desired scaling form $N_P(t;L) \sim \mathcal{N}(t/L^{\alpha_P})$ are observed for $t/L^{\alpha_P} \gtrsim 0.1$. These are indeed expected since the system enters the next dynamic regime of approach to full consensus. As u increases from zero, $\mathcal{N}(u)$ increases monotonically up to a certain value greater than 1. At this stage of the dynamics there are, then, states with more than one wrapping cluster. The scaling function next decreases

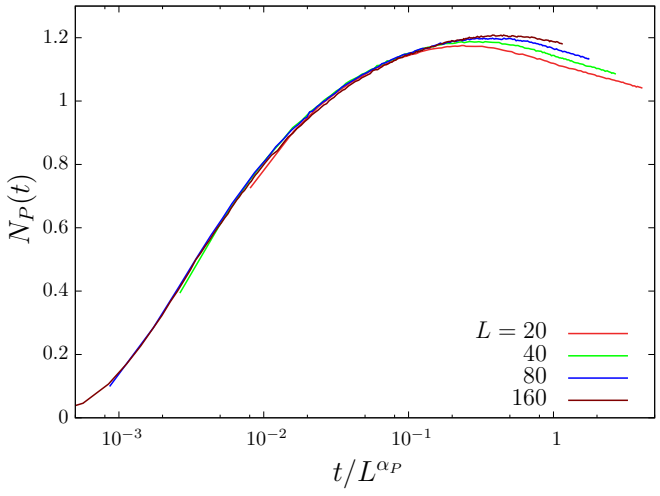

FIG. 9. (Color online) Average number of wrapping domains $N_P(t,L)$ against rescaled time t/L^{α_P}, with $\alpha_P = 1.667$, for systems of sizes $L = 20, 40, 80, 160$. As $t \to +\infty$ the curves should converge to 1 (single domain state).

converging to 1 from above. The exponent α_P sets the typical time required for the system to reach a regime with wrapping clusters to $t_P \sim L^{\alpha_P}$.

F. The largest cluster

We identified the largest cluster at each step of evolution and we computed several of its properties. This analysis allows us to distinguish whether the largest cluster has wrapped around the system in one or more directions and, moreover, to which kind of criticality it belongs.

We first measured the averaged number of its interfaces with positive, vanishing, and negative curvature, $\langle N_+\rangle$, $\langle N_0\rangle$, and $\langle N_-\rangle$, respectively. A nonpercolating cluster has a single external interface with positive curvature; we therefore call $\langle N_{\rm ep}\rangle = \langle N_+\rangle$ (with $_{\rm ep}$ for external perimeter). A cluster that percolates in one direction has two interfaces with vanishing curvature. The interfaces with negative curvature are internal to the cluster and surround its holes.

Another interesting observable is the area of the largest cluster A_c that we normalize as A_c/L^{D_A} with D_A a fractal dimension that we need to find. We recall that the fractal dimension of cluster areas in $2d$ site percolation [38,39] is

$$D_A^{\rm cp} \simeq 1.896. \tag{3.6}$$

Finally, we calculated the averaged total length of the boundary l_c as the sum of the length of external and internal interfaces described above. We also normalized this length as l_c/L^{D_H} with D_H a fractal dimension. For the sake of comparison, we recall that for $2d$ site percolation the cluster hull fractal dimension [40,41] takes the value

$$D_H^{\rm cp} = 1.750. \tag{3.7}$$

All these quantities show different scaling properties at short times before percolation is reached and at longer times, when the percolating cluster has established, and the further evolution takes the system to the final absorbing state. In the former time regime, the data scale as a function of t/L^{α_P} with $\alpha_P = 1.667$, see all panels in the right column in Fig. 10 , while in the latter they do as a function of t/L^2 (apart from logarithmic corrections), see all panels in the left column in the same figure. The value of α_P is rather large in the voter model (much larger than in the $2d$IM where $\alpha_P = 1/2$ [24]) and this makes the distinction between the regime of approach to percolation and the further evolution towards full consensus very hard.

The averaged number of interfaces with positive curvature smoothly decays from one to zero as more and more samples wrap around the sample in at least one direction, see Figs. 10(a) and 10(b). Concomitantly, the averaged number of maximal size clusters that wrap around the sample in one direction increases in time from zero initially to a value that is close to 0.9 to later decay again to zero when the cluster percolates in the other direction as well, leaving only internal interfaces in the system (not shown). The averaged number of internal boundaries has a very similar qualitative behavior to the one of the zero-curvature ones (not shown either). Panel (a) confirms the scaling with t/L^2 at long times while panel (b) indicates that the good scaling variable at short times is t/L^{α_P}.

Figures 10(c)–10(f) display the area of the maximum size cluster and the total perimeter length, respectively. The

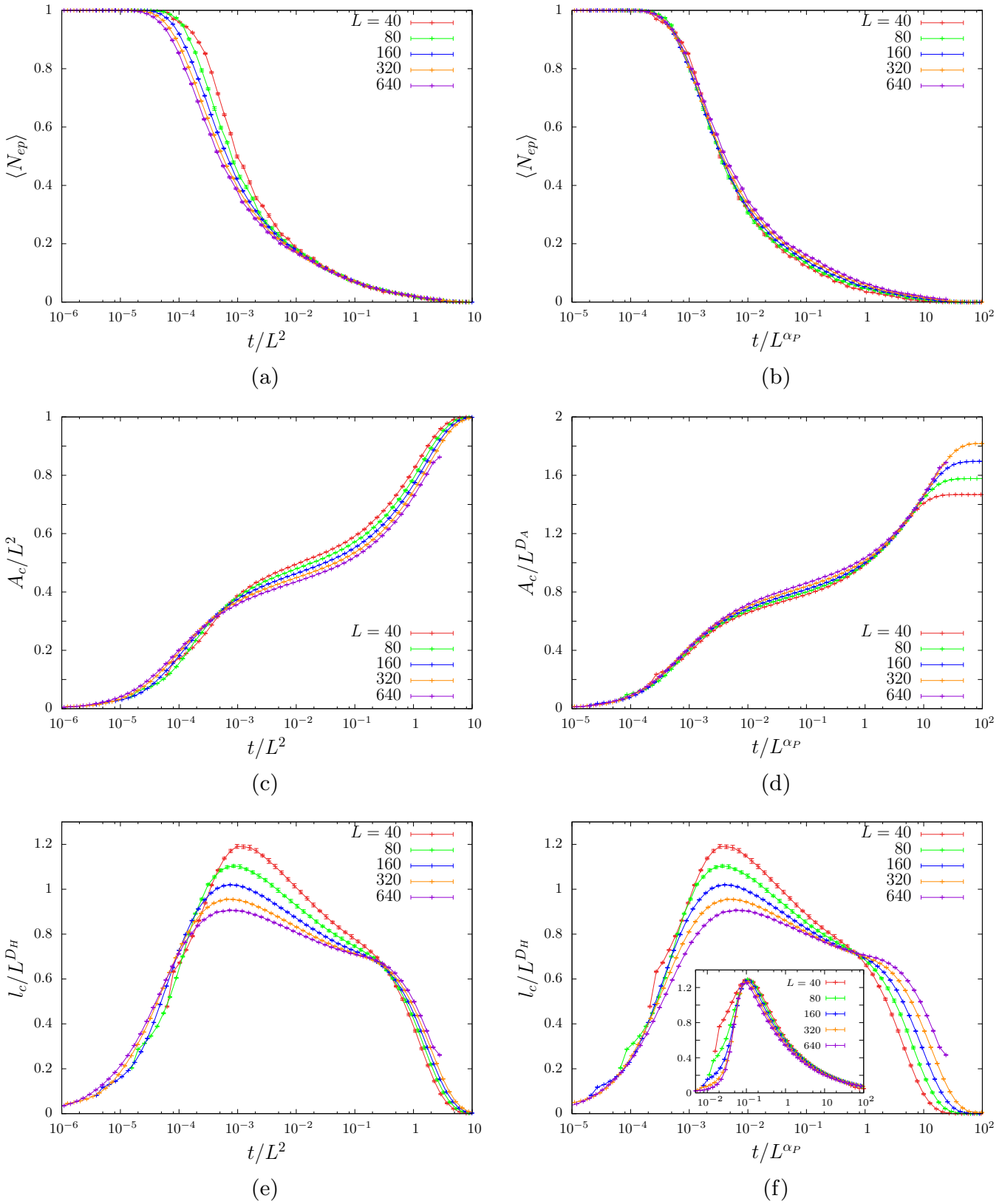

FIG. 10. (Color online) The largest cluster. The horizontal axes are t/L^2 and t/L^{α_P} with $\alpha_P = 1.667$ in all panels in the left and right columns, respectively. [(a) and (b)] The averaged number of external interfaces (only for nonpercolating clusters). Its area A_c normalized by L^2 in (c) and L^{D_A} with $D_A = 1.89583$ in (d). [(e) and (f)] Its total perimeter length in the voter and $2d$IM quenched to $T = 0$ (inset) normalized by L^{D_H} with $D_H = 1.75$.

asymptotic approach of A_c/L^2 in Fig. 10(c) to one and l_c in Fig. 10(e) to zero confirm that the systems approach full consensus. They also prove that there are no blocked states in the voter model as there are in the $2d$IM at $T = 0$ [42–46].

The scaling of the horizontal axis in Figs. 10(c) and 10(e) is intended to work at long times only. The persistent deviations from scaling should be due to the fact that we did not include in the scaling variable corrections that depend logarithmically on the system size, although we know from the analysis of the consensus time that these should exist.

The scaling of the vertical axis in Fig. 10(d) is intended to determine the fractal dimension of the area of the largest cluster, in the short-time regime. We used different values of D_A and we found that the most satisfactory collapse in the short-time regime is found for D_A in the interval 1.89–1.93. In Fig. 10(d) we show the scaling found using the fractal dimension of $2d$ critical site percolation, $D_A = D_A^{\rm cp} \simeq 1.89583$, which is within this interval (while D_A for other critical states lies outside this interval, i.e., $D_A^{\rm ci} = 1.948$ at the critical Ising point). Once again, due to the large value of α_P the two relevant asymptotic regimes are not well separated, and we cannot do better than this in the determination of D_A.

Similarly, the scaling of the vertical axis in Fig. 10(f) should determine the fractal dimension of the boundary of the largest cluster, D_H (although we stress that we show data for the total interface length here). Using $D_H = D_H^{\rm cp} = 1.75$ we see that all curves cross at $t/L^{\alpha_P} \simeq 1$ suggesting that critical percolation is reached at around $t_P \simeq L^{\alpha_P}$. Other choices for the value of D_H do not allow for data collapse at any value of the scaling variable. Furthermore, one could argue that the scaled data for t/L^{α_P} are slowly approaching, for increasing system size, a flat form.

In the inset to Fig. 10(f) we show, for comparison, the same scaling plot, l_c/L^{D_H} against t/L^{α_P}, for the zero temperature Ising model quenched from $T_0 \to \infty$, with $D_H = 1.75$ and $\alpha_P = 0.5$. Apart from the rather small system sizes, $L = 40$, 80, the data for the larger systems show a very good collapse over a rather large time window. In the Ising model the two asymptotic time regimes are rather well separated (as $\alpha_P = 0.5$ differs considerably from $z_d = 2$) and this fact contributes to the good data collapse.

G. Two growing lengths

We conclude that, as in the $2d$ Ising model with nonconserved order parameter [21–24], the dynamics of the finite-size $2d$ voter model takes place in two distinct regimes: The system first develops wrapping clusters of critical site percolation kind; once these are established, the further growth is a more usual coarsening process. The two growing lengths controlling the evolution in the two regimes are

$$\ell_P(t) \simeq t^{1/\alpha_P}, \quad \ell_G(t) \simeq t^{1/z_d}. \tag{3.8}$$

In the Ising model on a square lattice the exponents α_P and z_d differ, $\alpha_P = 1/2$ [24] and $z_d = 2$. Since α_P is so small, for the system sizes used in numerical simulations the approach to percolation occurs in a few steps and the time window is not sufficiently long to allow for a careful dynamic scaling analysis. Instead, in the voter model, $\alpha_P \simeq 1.667$ is quite large and does not differ much from $z_d = 2$. The system takes much longer to reach critical percolation and the advantage is that a rather wide time window can be explored in which the relevant growing length is $\ell_P(t)$.

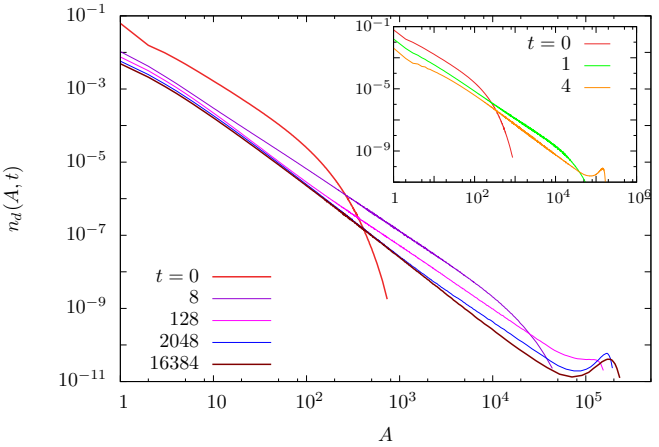

FIG. 11. (Color online) Instantaneous domain area number densities. Main plot: $2d$ voter model with linear size $L = 640$. Inset: $2d$IM quenched to $T = 0$ from $T_0 \to \infty$ and $L = 640$. In both cases the curves are presented in a double logarithmic scale and the times at which the data are collected are given in the key.

H. Density of domain areas

We now turn to the statistics of domain areas. We recall that we defined a cluster or a domain as the connected ensemble of nearest-neighbor parallel spins and its area as the number of spins in it.

Figures 11 shows raw data for the time-dependent number density of domain areas in systems with linear size $L = 640$. Initially, the curves show no particular structure, as the random initial condition is noncritical and the weight of the distribution at large areas drops significantly. However, as time elapses, a power law extending over several decades develops, as already noted by Scheucher and Spohn [11]. Moreover, a bump with support over areas that are of the order of magnitude of the size of the system also appears. These areas are the ones of clusters that wrap around the system, as the ones discussed in the previous subsection. The height of the bump increases in time. It tends to become stable at the longest time scales used, $t \simeq 17 \times 10^3$. (For a smaller system size, say $L = 160$, the same features are realized but, in contrast, after growing in height the bump tends to wash out after times of the order of 2×10^3.) This feature is very similar to what was observed in the $2d$IM quenched to zero temperature, although a stable bump, linked to the system reaching critical percolation, establishes at a much shorter time scale, $t_P \simeq 5$ for similar system sizes [21,22] as $\alpha_P = 1/2$ in this case [24]. Indeed, the curves for $t = 0$, 1, 4 in the inset are qualitatively identical to the ones for $t = 0$, 8,16384 in the main plot. (We will make a quantitative comparison between the behavior in the two models below.) In the case of the $2d$ voter model we observed that percolating clusters can appear in early stages of the dynamics, but they tend to break soon after their formation and reappear later on, taking longer to establish a stable pattern, see Fig. 2. In particular, for a system with linear size $L = 640$,

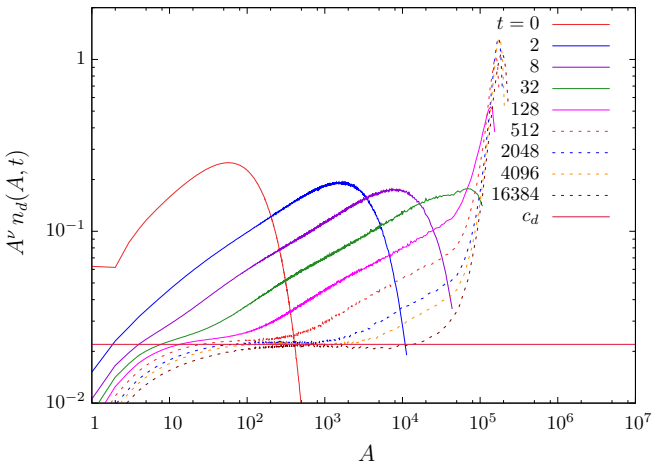

FIG. 12. (Color online) Time-dependent number density of domain areas, n_d, multiplied by A^ν with $\nu \simeq 1.98$ for $L = 640$. As the system comes closer to the percolating state, the number density of domain areas tends to the time-independent form $n_d(A,t) \sim c_d\ A^\nu$, save for a correction due to wrapping domains in the bump. The value of ν was estimated by fitting the aforementioned functional form to the data corresponding to the latest time. The horizontal line is at $c_d \approx 0.022$.

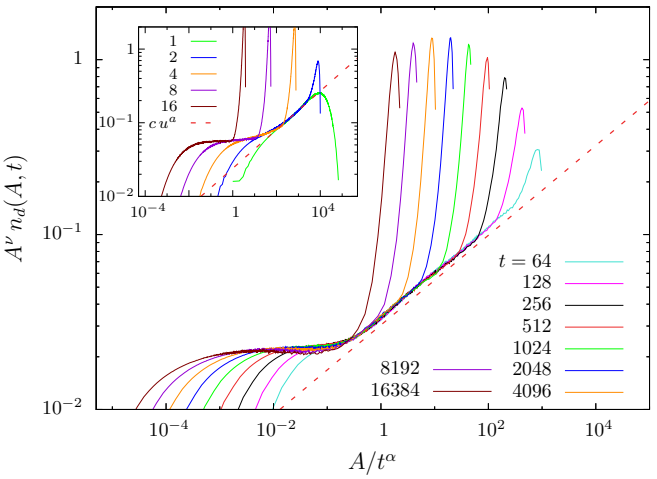

FIG. 13. (Color online) Number density of domain areas multiplied by A^ν against the rescaled area A/t^α for $L = 640$. The exponent ν takes the same values as in Fig. 12: $\nu \simeq 1.98$. The value of α that yields the best time scaling is $\alpha \simeq 1.19$. A fit to the function $f(u) = c\ u^a$ of the data at $t = 64$ over the interval $[1,100]$ yields $a \approx 0.26$. The red dashed line was added to better visualise this power-law behavior. Inset: The same scaling plot for the $2d$IM after a quench to $T = 0$, at five short times given in the key. The plateau is at $2c_d \simeq 0.044$ as explained in Ref. [21]. The power law shown with a dashed line was drawn with the same value of the exponent a as for the voter model.

a stable structure of percolating domains establishes only after a time of the order of $t_P \sim 10^5$.

The analytic and numeric analysis of the $2d$IM quenched from infinite to zero [21,22] or the critical [23] temperature showed that the number density of areas approaches a scaling form

$$A^\nu\, n_d(A,t) = \Phi\left[\frac{A}{\ell^{D_A}(t)}\right], \tag{3.9}$$

where D_A is the fractal dimension of the areas studied, $\ell(t)$ is the relevant growing length, and Φ a proper scaling function. After t_P this scaling has to be corrected by an additive term that takes into account the percolating clusters that had already established (the bump). In the zero-temperature quenches of the $2d$IM the approach to percolation was so fast that the study of this scaling for times such that the relevant growing length is $\ell_P(t)$ was not performed. In the critical quenches in [23] a triangular lattice for which the system was already at the critical percolation point initially was used. Here, with the voter model, we have the possibility of studying the dynamic scaling in the regime of slow approach to percolation in detail, by taking advantage of the large value of α_P.

The same data sets used in Fig. 11 are plotted in the form $A^\nu\, n_d(A,t)$ against A in Fig. 12 with $\nu \simeq 1.98$ for $L = 640$. The value of the exponent ν was found by fitting the data $n_d(A,t)$ corresponding to the longest time reached in the simulation ($t = 2048$ for $L = 160$, not shown, and $t = 16384$ for $L = 640$) with the power law $c_d A^{-\nu}$, in the range of areas $[10^2, 10^3]$ for $L = 160$ and $[10^2, 10^4]$ for $L = 640$. We found $c_d = 0.0207 \pm 0.0001$ and $\nu = 1.972 \pm 0.005$ in the case $L = 160$, and $c_d = 0.0220 \pm 0.0001$ and $\nu = 1.980 \pm 0.001$ for $L = 640$.

The value of the exponent ν increases very weakly with L and should be larger than 2 in the infinite-size limit to ensure that the average area of nonpercolating domains, $\int dA\ A\, n_d(A,t)$, is a finite quantity. However, the approach to the asymptotic limit is so slow that it is very hard to get closer to it numerically. This particular feature of the dynamics was also observed in Ref. [11] for the voter model and we stress that, in the $2d$IM, the expected value $\nu = 2.05$ is found only for a very careful choice of the areas to fit.

The value taken by the constant c_d is very relevant to our discussion. Indeed, it was used in Refs. [21,22] to distinguish the criticality of large-scale domains in zero-temperature quenches of the $2d$IM from equilibrium at $T_0 \to \infty$ and $T_0 = T_c$. More precisely, the area distribution of clusters of occupied sites at critical site percolation and, say, domains of positive spins at the critical Ising point are given by $n_d(A) \simeq 2C/A^{\tau^{\rm cp}}$ and $n_d(A,0) \simeq C/A^{\tau^{ci}}$, respectively, with $2C \simeq 0.023$, and $\tau^{\rm cp} = 1 + d/D_A^{\rm cp}$ and $\tau^{\rm ci} = 1 + d/D_A^{\rm ci}$ the Fisher exponents related to the fractal dimensions of the domain areas under the two critical conditions. Cardy and Ziff [47] obtained these universal constants analytically for the number density of *hull-enclosed* areas instead of *domain* areas using a Coulomb gas approach. Arguments presented in Ref. [22] suggest that very close values should apply to domain areas as well. Numerical simulations on the square and triangular lattice confirmed the value obtained with field-theoretic methods for hull-enclosed and domain areas [22,24,47]. After a zero-temperature quench of the $2d$IM with initial states drawn from infinite-temperature and critical-temperature conditions, the evolving large-scale areas are distributed algebraically and the number densities have Fisher exponents *and* constants in the numerator that are the ones cited above for critical site percolation (see the inset to Fig. 13) and critical Ising conditions, though both multiplied by a factor of 2 when clusters of both (up and down) species are counted [22].

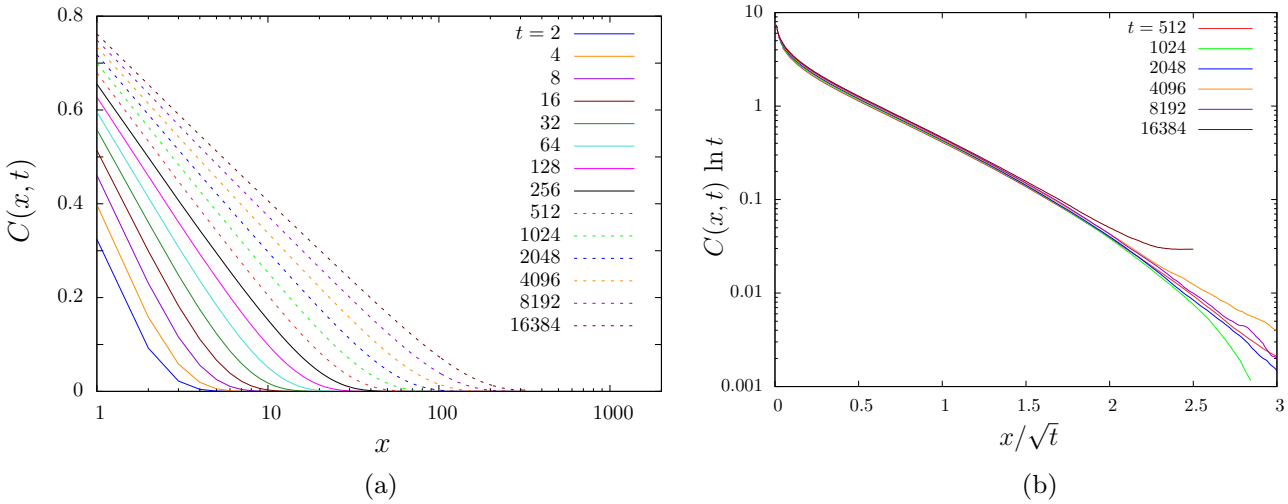

FIG. 14. (Color online) (a) Log-linear plot of the space-time correlation function along a principal direction of the lattice, i.e., $C(x,t) = \langle s_{x\mathbf{e}_i}(t) s_{\mathbf{0}}(t)\rangle$, at different times for a system with linear size $L = 640$. (b) The same data as in panel (a) multiplied by $\ln t$ and plotted against the scaled distance $x/\sqrt{t}$ in linear-log scale. See the main text for a discussion.

In the voter model with random initial conditions we find $c_d \simeq 0.022$ that is consistent with $c_d = 2C$ (within numerical accuracy), see Fig. 11, and with critical Ising initial configurations we find a constant taking the value $c_d/2 = C$ (not shown). This result confirms the reduction of the number density of finite areas by two for initial conditions with long-range correlations with respect to the ones with only short-range correlations.

In Fig. 13 we show $A^{\nu}\, n_d(A,t)$ against the rescaled area A/t^{α} for systems with $L = 640$. The value of α that allowed us to obtain the best collapse was found to be approximately equal to 1.19. This value is in good agreement with the prediction $\ell_P^{D_A}(t) \simeq t^{D_A/\alpha_P} = t^{1.90/1.67} = t^{1.14}$. In the inset we perform the same analysis on the $2d$IM quenched to $T = 0$, by focusing on the very short time dynamics such that $t \ll t_P$. In agreement with the proposal, the curves collapse if one uses $A/t^{D_A/\alpha_P} = A/t^{(187/96)/0.5} = A/t^{3.9}$.

Apart from deviations caused by the appearance of wrapping domains in the bump, for large values of t all curves seem to have the same behavior, namely two distinct regimes: For $A/t^{\alpha} \lesssim 0.1$ there is a nearly flat region, which would mean that $\Phi(u) \sim$ const and thus $n_d(A,t) \sim A^{-\nu}$, i.e., the statistics of domain areas is independent of time; for $A/t^{\alpha} \gtrsim 0.1$ instead, the scaling function seems to behave as an increasing power law $\Phi(u) \sim c\, u^a$, with a self-similar statistics of domain areas in the sense that it depends only on A/t^{α}. A fit of the data for the shortest time in Fig. 13 on the interval [1,100] of the scaling variable $u = A/t^{\alpha}$, yields $c = 0.034 \pm 0.001$ and $a = 0.257 \pm 0.001$. Analogously, for the case $L = 160$ we obtained $c = 0.032 \pm 0.001$ and $a = 0.264 \pm 0.001$ (not shown). The existence of two distinct regimes for small and large values of A/t^{α} is also observed in the Ising model as shown in the inset of Fig. 13. Moreover, for large values of A/t^{α} we also observe an increasing power law (also shown in the inset) with a very similar power, i.e., $c = 0.024 \pm 0.001$ and $a = 0.262 \pm 0.001$ for $L = 640$.

Coming back to the domain area statistics, as one can see from the plots, the flat region for $A/t^{\alpha} \lesssim 0.1$ becomes larger as time increases, while the complementary region of larger domains shrinks, until disappearing. Note that as time increases the percolating (wrapping) domains become more and more predominant and eventually the number domain density converges to the absorbing state form which is just a δ function centered at $A = L^2$. Even though this fact does not rule out the possibility of a transient regime in which more than one stable percolating clusters coexist, similarly to what happens in the zero-temperature $2d$IM on a finite lattice, we found that it establishes during a very short time period (compared to the whole duration of the dynamics) before the consensus state is reached, so it is somehow difficult to "catch" it in the domain area statistics.

I. Space-time correlation function

Having established the existence of two dynamic growing lengths in a finite-size system, we now put the scaling form of the space-time correlation, Eq. (2.18), to the numerical test. Figure 14(a) shows data for $C(r,t)$ on a lattice of linear size $L = 640$. The correlation function was calculated only along a principal direction of the lattice (e.g., the horizontal direction), as $C(\boldsymbol{x},t)$ should be isotropic and depend on $|\boldsymbol{x}|$ only at distances much longer than the lattice spacing. In Fig. 14(b) the correlation function multiplied by $\ln t$ is plotted against the scaled distance $x/\sqrt{t}$. The curves at different times tend to collapse even though they deviate for large values of $x/\sqrt{t}$. These deviations are due to finite-size effects: Since we have taken periodic conditions at the boundaries, the data at distances of the order of the lattice size, specifically $x \simeq L/2$, are much affected by the boundaries. One reckons that, consistently, the deviation from the scaling law for large $x/\sqrt{t}$ occurs at smaller values of the scaling variable at longer times.

However, from the analysis of the clusters we now known that in the dynamic regime in which percolating clusters develop there is another characteristic length in the problem, $\ell_P(t)$. Accordingly, the scaling form of the correlation

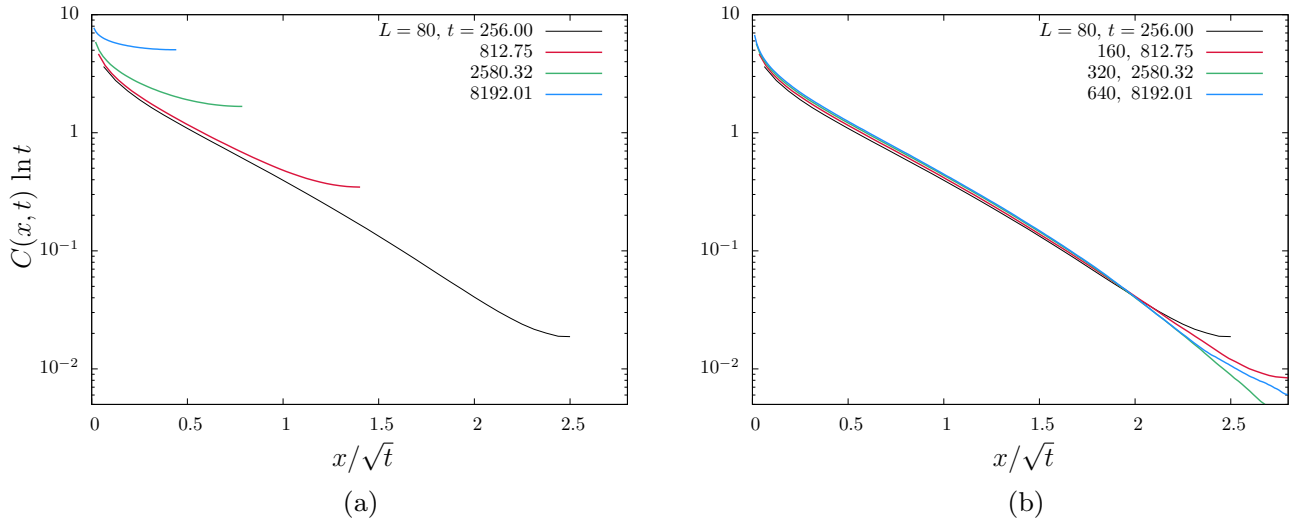

FIG. 15. (Color online) $C(x,t)\ \ln t$ against scaled distance $x/t^{1/z_d}$ with $z_d = 2$ the dynamical exponent in a linear-log plot. In panel (a) data are for $L = 80$ at different times given in the key. Panel (b) reports data for different L_i and the corresponding times t_i such that $L_i^{\alpha_P}/t_i$ is held constant. $\alpha_P \approx 1.667$ is the exponent in the relation $t_P \sim L^{\alpha_P}$, with t_P the time needed for stable percolating domains to establish (see Sec. III F for more details on t_P).

function has to be modified to capture the dynamics in both dynamic regimes (see Ref. [24] for this analysis in the $2d$IM). We therefore introduce a new two-variable scaling function $g(u,v)$,

$$C(\boldsymbol{x},t;L) = \frac{1}{\ln(t/\tau)}\, g\left[\frac{|\boldsymbol{x}|}{\ell_G(t/\tau)}, \frac{\ell_P(t/\tau)}{L}\right], \qquad (3.10)$$

such that for $t \simeq t_P \simeq L^{\alpha_P}$, the new scaling variable is close to 1, $\ell_P(t)/L \simeq 1$, and one recovers the infinite-size limit. This suggests that the data for $C(x,t;L)$ at different times t_i and sizes L_i, chosen in a such a way that the ratio $\chi = \ell_P(t_i)/L_i$ is kept constant, should collapse when plotted against the scaled distance $x/\ell_G(t) \simeq x/\sqrt{t}$, since $z_d = 2$ in the voter model. In order to put this proposal to the test we computed the correlation function on square lattices with sizes $L_i = 2^i L_0$ for $L_0 = 80$ and $i = 0$ - 4 and times $t_i = 2^{i\,\alpha_P} t_0$, with $t_0 = 256$, such that $\chi = t_0^{1/\alpha_P}/L_0$. As far as the exponent α_P is concerned, we estimated it from the analysis of the largest cluster obtaining $\alpha_P \approx 1.667$, see Sec. III F, and we confirmed its value with the study of the time evolution of the number of percolating domains, see Sec. III E.

Figures 15(a) and 15(b) present the scaling forms in Eqs. (2.18) and (3.10), respectively. It is clear that the introduction of an extra scaling variable with the dependence on the new length scale allows us to achieve a much better data collapse.

IV. CONCLUSIONS

The main goal of this work was to improve the understanding of coarsening in models with microscopic dynamics that are not driven by the minimisation of a thermodynamic potential and do not satisfy detailed balance. More precisely, we focused on a $\mathbb{Z}_2$-symmetric lattice model with pairwise interactions driven by interfacial noise, *viz.* the $2d$ linear voter model on a square lattice.

We showed that the dynamic evolution of the bidimensional voter model on a square lattice proceeds in two distinct dynamic regimes. In the first one, the model approaches critical site percolation. The time needed to reach one such typical state diverges with the size of the system algebraically, $t_P \simeq L^{1/\alpha_P}$, with the exponent $\alpha_P \simeq 1.667$ that is much larger than the one previously evaluated in the $2d$IM quenched to $T = 0$ [23]. Next, the model evolves following a different mechanism in which consensus is progressively attained. The characteristic growing length for this process is also algebraic, $\ell(t) \simeq t^{1/z_d}$, though with a different dynamic exponent, $z_d = 2$. In the social dynamics context, the first process can have important consequences.

We based the conclusions above on the careful use of numerical methods. We first tested this approach against the theoretical predictions that were already available for the infinite-size voter model. Most of the computed quantities, such as the fraction of active interfaces, the autocorrelation function, and the persistence, were found to be in very good agreement with the analytic predictions for infinite-size systems. In particular, the peculiar logarithmic decay of the magnitude of the two-body correlation function and of the fraction of active interfaces was recovered, even though these results could be improved by simulating larger systems on very long times. We then focused on the spin configurations and from the analysis of their statistical and geometric properties we uncovered the approach to critical site percolation. Once the new growing length scale identified, we used it to improve the scaling of the space-time correlation function for finite-size systems.

In a series of papers, the role played by the approach to critical percolation in spin models with Ising [21–24,48,49] or Potts [50,51] variables in two or three dimensions [52] was studied. In all these cases the dynamics satisfy detailed balance and eventually take a finite-size system to thermal equilibrium. In this paper we explored a different kind of microscopic dynamics that does not satisfy detailed balance and approaches

an absorbing state asymptotically. We still found a similar approach to critical percolation as in the "equilibrium" cases albeit with a much slower growing length.

In Ref. [24] we observed that for the Ising model with microscopic dynamics satisfying detailed balance the exponent α_P coincided with the ratio between the dynamic exponent for the late stage growth, z_d, and the lattice regular or averaged coordination number, n_c, i.e., $\alpha_P = z_d/n_c$. In the voter model the dynamic exponent is $z_d = 2$ (on top, dynamic scaling for infinite-size systems suffers from logarithmic corrections) and, though a coordination number cannot be really identified, we can claim that an effective one is somehow larger than 1. With this identification, the value of α_P found numerically has the good trend, in the sense that the coordination number is smaller than in Ising and this leads to a larger α_P.

This works opens several lines for future research. On the one hand, it would be interesting to extend this analysis to different types of lattices, variants of the update rule (with, e.g., noise [12], local conservation laws [53], memory [54], or inhomogeneities in the form of zealots [55]) and upgrading the voters to have many opinions (see Ref. [56] and references therein). On the other hand, it should be possible to extract the growing length $\ell_P(t)$ analytically by taking into account the finite-size effects in the approach explained in Sec. II.

ACKNOWLEDGMENTS

We thank H. Hinrichsen for an early discussion on this model that motivated this study. L.F.C. received partial support from Institut Universitaire de France.

[1] C. Castellano, S. Fortunato, and V. Loreto, Rev. Mod. Phys. **81**, 591 (2009).
[2] D. Tilman and P. Kareiva, eds., *Spatial Ecology: The Role of Space in Population Dynamics and Interspecific Interactions* (Princeton University Press, Princeton, NJ, 1997).
[3] P. Clifford and A. Sudbury, Biometrika **60**, 581 (1973).
[4] R. A. Holley and T. M. Liggett, Ann. Probab. **3**, 643 (1975).
[5] T. M. Liggett, *Stochastic Interacting Systems: Contact, Voter and Exclusion Processes* (Springer, Berlin, 1999).
[6] P. L. Krapivsky, Phys. Rev. A **45**, 1067 (1992).
[7] P. L. Krapivsky, J. Phys. A **25**, 5831 (1992).
[8] L. Frachebourg and P. L. Krapivsky, Phys. Rev. E **53**, R3009 (1996).
[9] F. Vazquez, P. L. Krapivsky, and S. Redner, J. Phys. A **36**, L61 (2003).
[10] J. Fernández-Gracia, K. Suchecki, J. J. Ramasco, M. San Miguel, and V. M. Eguiluz, Phys. Rev. Lett. **112**, 158701 (2014).
[11] M. Scheucher and H. Spohn, J. Stat. Phys **53**, 279 (1988).
[12] M. J. de Oliveira, Phys. Rev. E **67**, 066101 (2003).
[13] J. T. Cox and D. Griffeath, Ann. Prob. **14**, 347 (1986).
[14] A. J. Bray, Adv. Phys. **43**, 357 (1994).
[15] S. Puri, in *Kinetics of Phase Transitions*, edited by S. Puri and V. Wadhawan (Taylor & Francis Group, London, 2009).
[16] L. F. Cugliandolo, Compt. Rend. Phys. **16**, 257 (2015).
[17] I. Dornic, H. Chaté, J. Chave, and H. Hinrichsen, Phys. Rev. Lett. **87**, 045701 (2001).
[18] L. Dall'Asta and C. Castellano, Europhys. Lett. **77**, 60005 (2007).
[19] P. C. Hohenberg and B. I. Halperin, Rev. Mod. Phys. **49**, 435 (1977).
[20] P. Calabrese and A. Gambassi, J. Phys. A **38**, R133 (2005).
[21] J. J. Arenzon, A. J. Bray, L. F. Cugliandolo, and A. Sicilia, Phys. Rev. Lett. **98**, 145701 (2007).
[22] A. Sicilia, J. J. Arenzon, A. J. Bray, and L. F. Cugliandolo, Phys. Rev. E **76**, 061116 (2007).
[23] T. Blanchard, L. F. Cugliandolo, and M. Picco, J. Stat. Mech. (2012) P05026.
[24] T. Blanchard, F. Corberi, L. F. Cugliandolo, and M. Picco, Europhys. Lett. **106**, 66001 (2014).
[25] Frachebourg and Krapivsky [8] define the spin-flip rate with a factor $1/\tau$ in front of the parenthesis, they take $\tau = 4/d$, and they therefore have an overall factor $d/4$. This coincides with our definition of W_x since we have a factor $1/(2\tau)$, we choose $\tau d = 2$ and we also have a factor $d/4$ overall. There is, however, a difference with the choice made by Ben-Naim *et al.*, who used a τ that is half ours in their calculations [27].
[26] J.-M. Drouffe and C. Godrèche, J. Phys. A **32**, 249 (1999).
[27] E. Ben-Naim, L. Frachebourg, and P. L. Krapivski, Phys. Rev. E **53**, 3078 (1996).
[28] F. Sastre, I. Dornic, and H. Chaté, Phys. Rev. Lett. **91**, 267205 (2003).
[29] J. T. Cox and R. Durrett, Bernoulli **1**, 343 (1995).
[30] J. Olejarz, P. L. Krapivsky, and S. Redner, Phys. Rev. E **83**, 051104 (2011).
[31] J. Olejarz, P. L. Krapivsky, and S. Redner, Phys. Rev. E **83**, 030104 (2011).
[32] P. Meakin and D. J. Scalapino, J. of Chem. Phys. **87**, 731 (1987).
[33] J. W. Evans and T. R. Ray, Phys. Rev. E **47**, 1018 (1993).
[34] J. W. Evans, Rev. Mod. Phys. **65**, 1281 (1993).
[35] A. J. Bray, S. N. Majumdar, and G. Schehr, Adv. Phys. **62**, 225 (2013).
[36] T. Blanchard, L. F. Cugliandolo, and M. Picco, J. Stat. Mech. (2014) P12021.
[37] M. Howard and C. Godrèche, J. Phys. A **31**, L209 (1998).
[38] D. Stauffer and A. Aharony, *Introduction To Percolation Theory* (Taylor & Francis, London, 1994).
[39] A. A. Saberi, Phys. Rep. **578**, 1 (2015).
[40] H. Saleur and B. Duplantier, Phys. Rev. Lett. **58**, 2325 (1987).
[41] A. Coniglio, Phys. Rev. Lett. **62**, 3054 (1989).
[42] V. Spirin, P. L. Krapivsky, and S. Redner, Phys. Rev. E **63**, 036118 (2001).
[43] V. Spirin, P. L. Krapivsky, and S. Redner, Phys. Rev. E **65**, 016119 (2002).
[44] K. Barros, P. L. Krapivsky, and S. Redner, Phys. Rev. E **80**, 040101 (2009).
[45] J. Olejarz, P. L. Krapivsky, and S. Redner, Phys. Rev. Lett. **109**, 195702 (2012).
[46] T. Blanchard and M. Picco, Phys. Rev. E **88**, 032131 (2013).
[47] J. Cardy and R. M. Ziff, J. Stat. Phys. **110**, 1 (2003).
[48] A. Sicilia, J. J. Arenzon, A. J. Bray, and L. F. Cugliandolo, Europhys. Lett. **82**, 10001 (2008).

[49] A. Sicilia, Y. Sarrazin, J. J. Arenzon, A. J. Bray, and L. F. Cugliandolo, Phys. Rev. E **80**, 031121 (2009).
[50] M. P. O. Loureiro, J. J. Arenzon, L. F. Cugliandolo, and A. Sicilia, Phys. Rev. E **81**, 021129 (2010).
[51] M. P. O. Loureiro, J. J. Arenzon, and L. F. Cugliandolo, Phys. Rev. E **85**, 021135 (2012).
[52] J. J. Arenzon, L. F. Cugliandolo, and M. Picco, Phys. Rev. E **91**, 032142 (2015).
[53] F. Caccioli, L. Dall'Asta, T. Galla, and T. Rogers, Phys. Rev. E **87**, 052114 (2013).
[54] H.-U. Stark, C. J. Tessone, and F. Schweitzer, Phys. Rev. Lett. **101**, 018701 (2008).
[55] M. Mobilia, Phys. Rev. Lett. **91**, 028701 (2003).
[56] M. Starnini, A. Baronchelli, and R. Pastor Satorras, J. Stat. Mech. (2012) P10027.